Electronic Supplementary Material (ESI) for Environmental Science: Nano.

Supporting Information For:

A Superhydrophobic Nanocrystalline MOF Embedded Starch@Cotton Composite for Fast, Selective and Nanomolar Sensing and Adsorptive Removal of a Fluorinated Herbicide from Aqueous Medium

*Subhrajyoti Ghosh, Paltan Laha and Shyam Biswas**

Department of Chemistry, Indian Institute of Technology Guwahati, 781039 Assam, India

*Corresponding author. Tel: 91-3612583309, Fax: 91-3612582349

E-mail address: sbiswas@iitg.ac.in

Materials and Characterization Methods:

All the reagents, starting materials and solvents were procured from commercial sources and used without purification, except the 2-(perfluorobenzamido)terephthalic acid linker. The linker was synthesized according to the below mentioned procedure (Scheme S1) and its purity was verified by the ATR-IR, ^{1}H NMR, ^{19}F NMR,^{13}C NMR and mass spectrometric analysis (Figures S1-S4). The notations used for characterization of the bands are broad (br), strong (s), very strong (vs), medium (m), weak (w) and shoulder (sh). Powder XRD analysis was executed by using Rigaku Smartlab X-ray diffractometer with Cu-*K*α radiation (λ = 1.54056 Å), 40 kV of operating voltage and 125 mA of operating current. The Attenuated Total Reflectance Infrared (ATR-IR) spectra were recorded using PerkinElmer UATR Two at ambient condition in the region 500-4000 cm^{-1}. Thermogravimetric analysis (TGA) was carried out with a PerkinElmer TGA 4000 thermogravimetric analyser in the temperature range of 30-700 °C under O_2 atmosphere at the rate of 4 °C min^{-1}. N_2 sorption isotherms were recorded by using Quantachrome Autosorb iQ-MP volumetric gas adsorption equipment at -196 °C. Before the sorption analysis, the degassing of the compound was carried out at 100 °C under a high vacuum for 24 h. FE-SEM images were captured with a Zeiss (Zemini) scanning electron microscope. A Bruker Avance III 500 NMR spectrometer was used for recording ^{1}H NMR and ^{19}F NMR spectra at 500 MHz. Fluorescence lifetimes were measured using Picosecond Time-resolved and Steady State Luminescence Spectrometer on an Edinburg Instruments Lifespec II & FSP 920 instrument. Fluorescence sensing studies were performed with a HORIBA JOBIN YVON Fluoromax-4 spectrofluorometer. Pawley refinement was carried out using Materials Studio software. The DICVOL program incorporated within STOE's WinXPow software package was used to determine the lattice parameters.

Synthesis Procedure of 2-(Perfluorobenzamido)Terephthalic Acid Linker:

For the synthesis of the 2-(perfluorobenzamido)terephthalic acid linker, in a two-necked round bottom flux (containing 15 mL of dry THF), 182 mg (1 mmol) of 2-aminoterephthalic acid was added and it was dissolved by sonication. Thereafter, 255 µL (1.1 mmol) of 2,3,4,5,6-pentafluorobenzoyl chloride was dropwise added to the aforementioned mixture under stirring conditions at room temperature. After the addition of 255 µL of 2,3,4,5,6-pentafluorobenzoyl chloride, the mixture was stirred for 2 h at room temperature under N_2 atmosphere (Scheme S1). After 2 h, a white coloured precipitate appeared. Then, the solvent was evaporated and the obtained white coloured product was dried for 12 h in an 80 °C oven. Yield: 360 mg (0.93 mmol, 96%). ^{1}H NMR (500 MHz, DMSO-d_6): δ = 11.73 (s, 1H), 8.98 (s, 1H), 8.10 (d, 1H), 7.80 (d, 1H) ppm. ^{13}C NMR (125 MHz, DMSO-d_6): δ = 169.53, 168.93, 166.73, 156.55, 151.63, 145.24, 145.18, 145.12, 143.59, 143.53, 143.47, 141.87, 141.77, 140.23, 140.13, 139.30, 139.21, 135.78, 131.85, 125.19, 122.15, 118.03, 115.98, 113.01, 110.04, 109.92, 109.08 ppm. ^{19}F NMR -141.57, -151.32, -160.95. MALDI-TOF (m/z): 398.196 for $(M+Na)^+$ ion (M = mass of 2-(perfluorobenzamido)terephthalic acid linker). In Figs. S1-S4, the NMR and mass spectra of the 2-(perfluorobenzamido)terephthalic acid linker are shown.

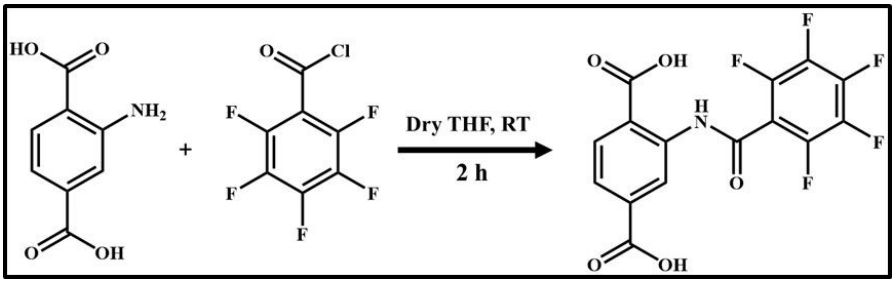

Scheme S1. Reaction scheme for the preparation of 2-(perfluorobenzamido)terephthalic acid linker.

Preparation of MOF (1′) Suspension for Fluorescence Sensing Experiments:

The probe **1′** (4 mg) was taken in a 5 mL glass vial containing 4 mL of methanol. Then, the suspension was sonicated for 15 min and kept it for overnight to make it stable. During the fluorescence sensing experiments, 200 µL of above-mentioned suspension of **1′** was added to 3000 µL of mixture of methanol and deionized water (volume ratio of water and methanol was 1:2) in a quartz cuvette. All the fluorescence spectra were collected in the range of 370-600 nm by exciting the suspension at 350 nm. For competitive experiments, the solutions of the different competitive analytes (concentration = 10 mM) were added to the suspension of **1′** and fluorescence spectra were collected in the same range.

Fabrication of MOF@Starch@Cotton Composite:

To fabricate the composite, initially, 300 mg of starch was heated under stirring conditions in 10 mL of water at 140 °C until the solution became clear. After preparing this homogeneous starch solution, 200 mg of solid MOF was added to it and the mixture was sonicated for 30 min to disperse the MOF particles homogeneously in the polymeric solution. After that, ten pieces (1 ×1 cm^2) of cotton fabric were dipped into the suspension and then it was dried in a 120 °C oven. This process was repeated three times to coat the polymeric solution uniformly.

Analysis of Band Gap:

For **1′**: E_g = 3.99 eV (calculated from the Tauc plot, Fig. S67a)

E_{VB} = Width of the He I UPS spectra from the excitation energy (21.22 eV)

E_{VB} = 21.22 - (16.22 – 2.87) = 7.87 eV

$E_{CB} = E_{VB} - E_g$ = 3.88 eV

With respect to RHE:

E_{VB} = 7.87 – 4.44 = 3.43 V

E_{CB} = 3.88 - 4.44 = -0.56 V

For trifluralin: E_g = 2.22 eV (calculated from the Tauc plot, Fig. S67b)

E_{VB} = Width of the He I UPS spectra from the excitation energy (21.22 eV)

E_{VB} = 21.22 - (17.90 – 7.96) = 9.94 eV

$E_{CB} = E_{VB} - E_g$ = 7.72 eV

With respect to RHE:

E_{VB} = 9.94 - 4.44 = 5.50 V

E_{CB} = 7.72 - 4.44 = 3.28 V

Details of Theoretical Calculations:

The electronic properties of MOF are mainly contributed by the corresponding linker of the MOF. Thus, for the simplicity of theoretical calculations, we adopted the optimized structure of the linker for TDDFT. Herein, the TDDFT calculations were performed with B3LYP functional and 6-311+G (d,p) basis sets in the gas phase with the help of Gaussian 09.[1] The TDDFT calculation of vertical excitation of the singlet state allows us to generate theoretical UV-Vis absorption profile which is displayed in Figure S40. Using GaussSum 3.0 software, the information related to transition wavelength (nm), oscillator strength (f), and associated molecular orbitals are extracted from the TDDFT output file (Table S6). The theoretically obtained excitation wavelength from the TDDFT is closely similar to the obtained experimental result for MOF (Table S6). To predict the fluorescence, we optimized the excited state geometries of the linker where we found that vertical emission energy at 394 nm and its associated oscillator strength (*f*) is 0.113.

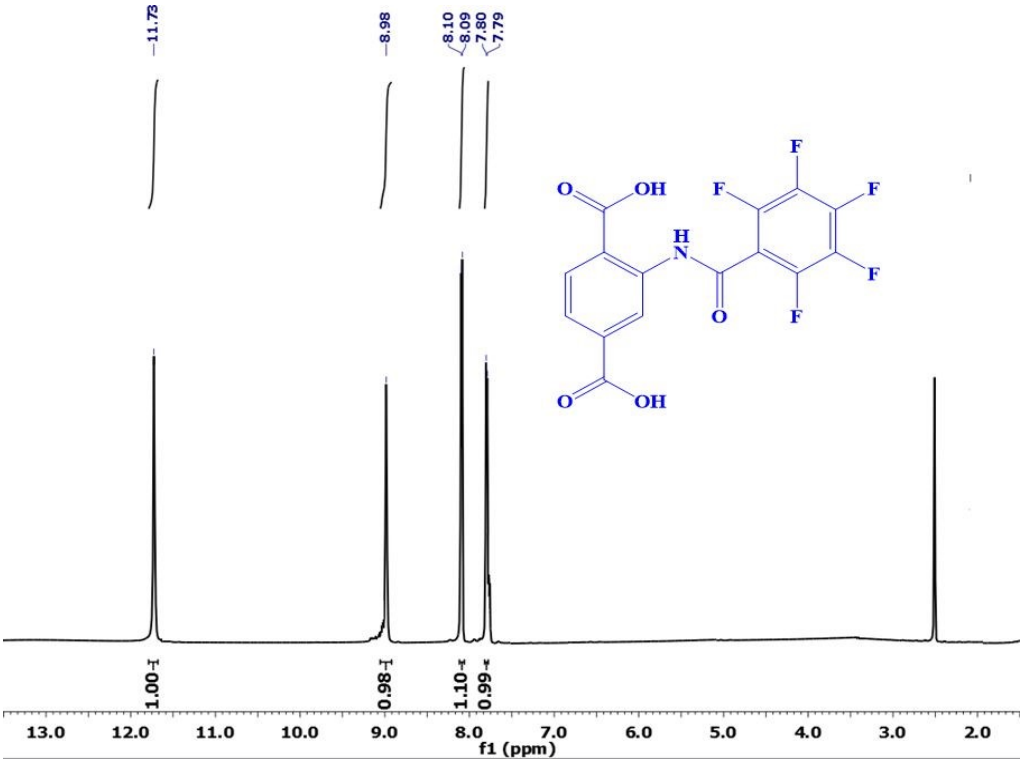

Fig. S1. ^{1}H NMR spectrum of 2-(perfluorobenzamido)terephthalic acid linker in DMSO-d_6.

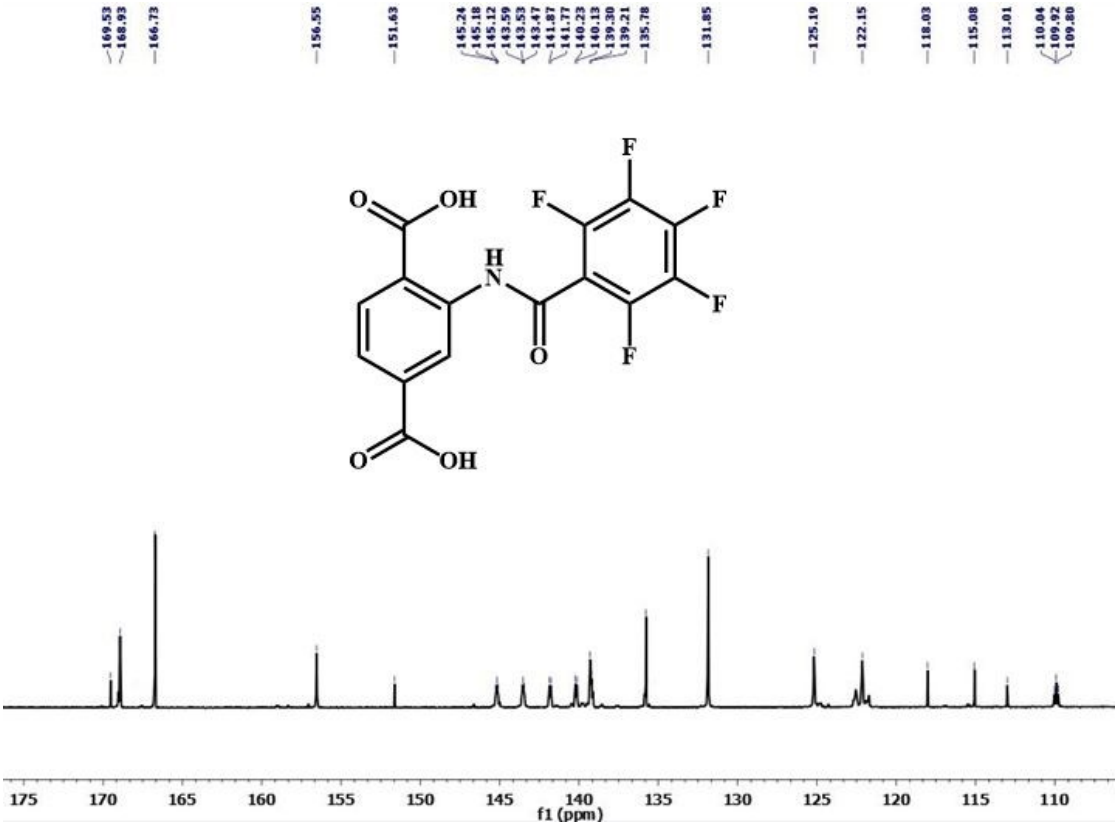

Fig. S2. ^{13}C NMR spectrum of 2-(perfluorobenzamido)terephthalic acid linker in DMSO-d_6.

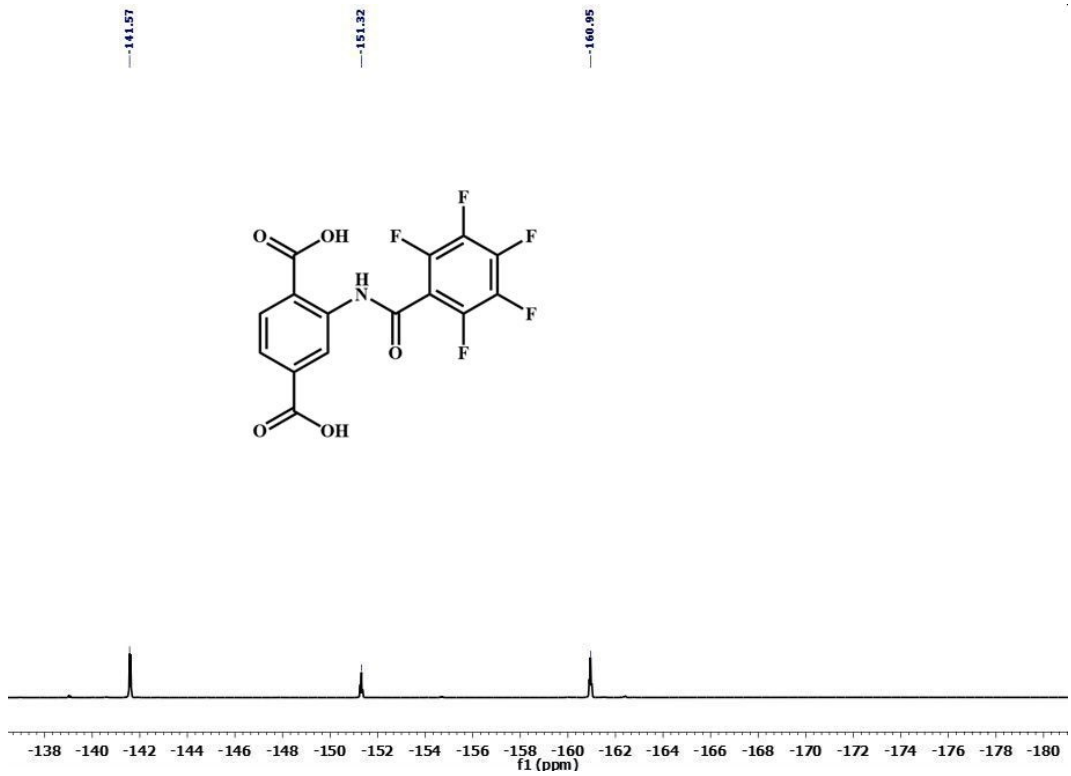

Fig. S3. ^{19}F NMR spectrum of 2-(perfluorobenzamido)terephthalic acid linker in DMSO-d_6.

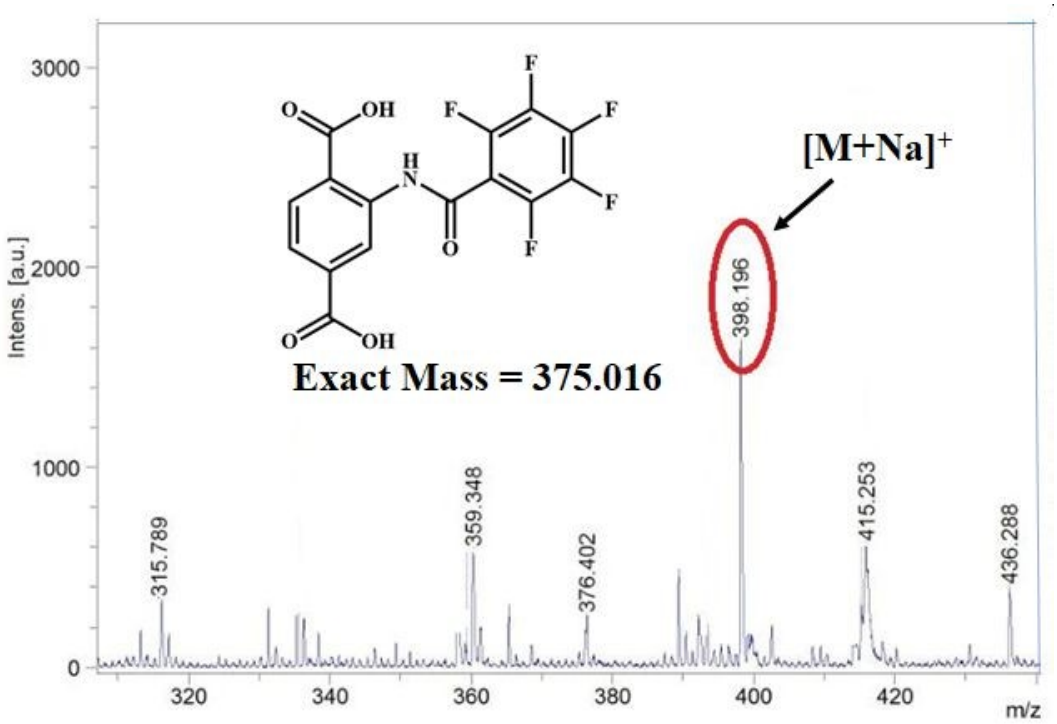

Fig. S4. MALDI-TOF mass spectrum of 2-(perfluorobenzamido)terephthalic acid linker measured in methanol. The spectrum shows m/z peak at 398.198, which corresponds to $(M+Na)^+$ ion (M = mass of 2-(perfluorobenzamido)terephthalic acid linker).

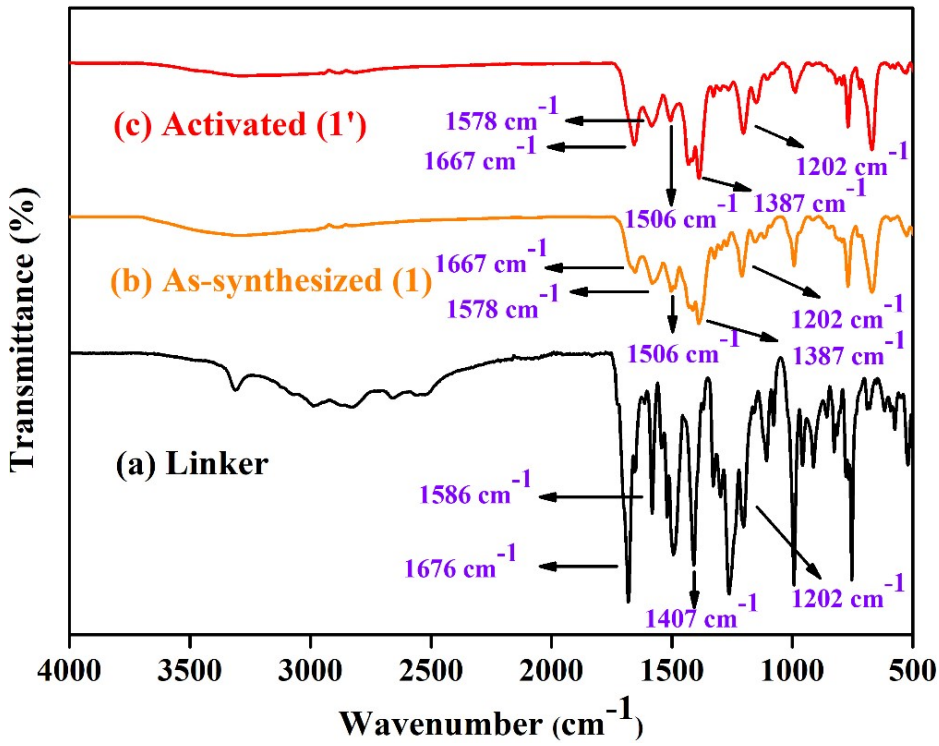

Fig. S5. ATR-IR spectra of (a) 2-(perfluorobenzamido)terephthalic acid linker, (b) **1** (as-synthesized) and (c) **1′** (activated).

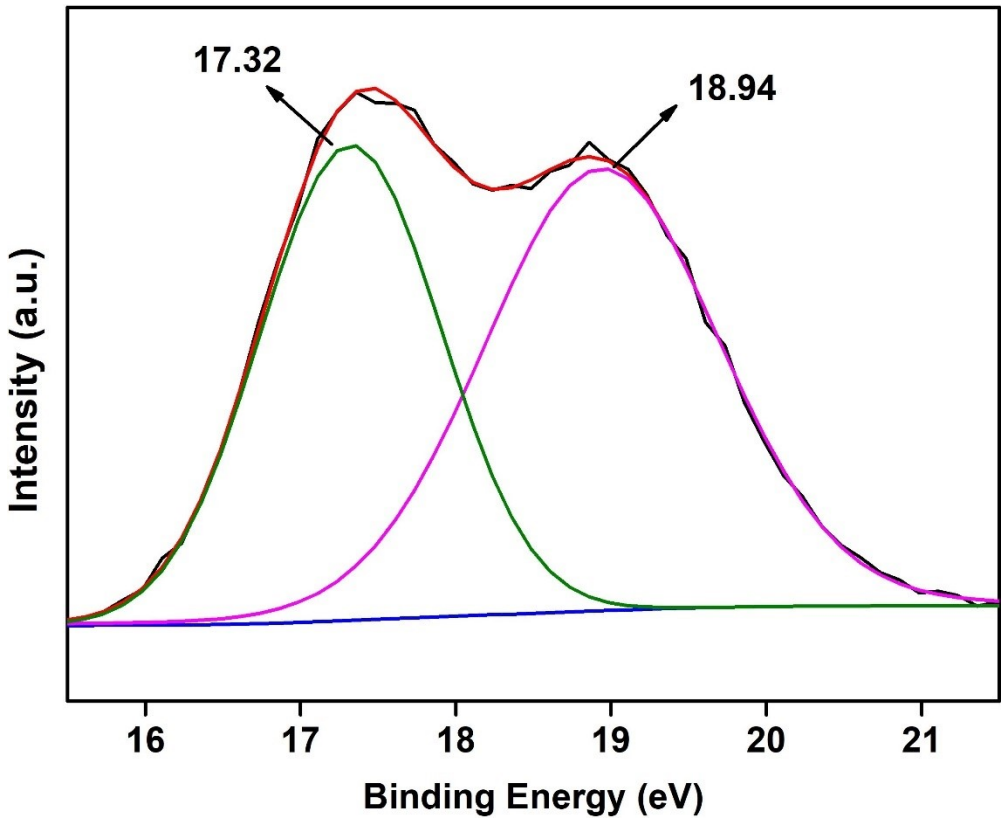

Fig. S6. Fitted XPS spectra of Hf (4f) of **1′**.

Table S1. Unit cell parameters of **1′** obtained by indexing its PXRD data. The obtained values have been compared with parent UiO-66 MOF.

Compound Name	**1′**	UiO-66[2]
Crystal System	cubic	cubic
a = b = c (Å)	20.785 (4)	20.7004 (2)
V (Å^3)	8979.4 (27)	8870.3 (2)

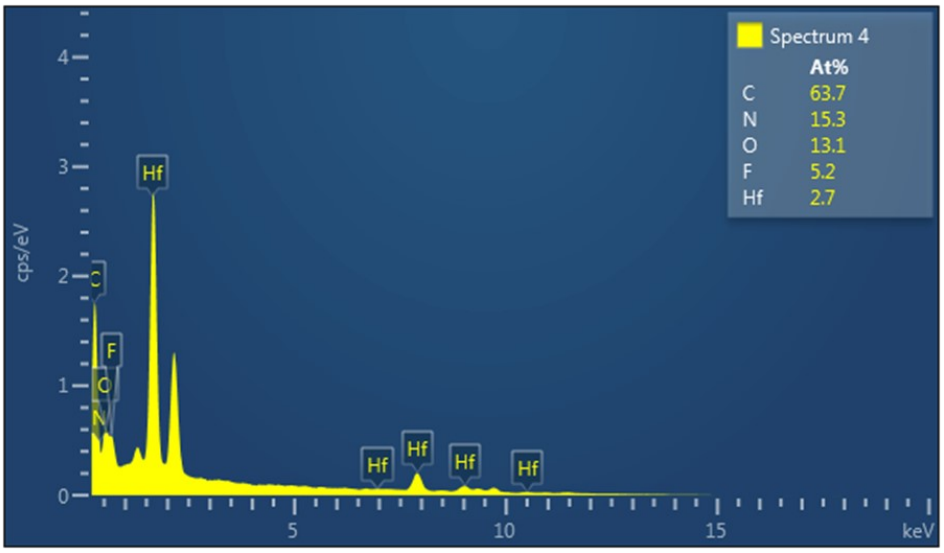

Fig. S7. EDX spectrum of **1′**.

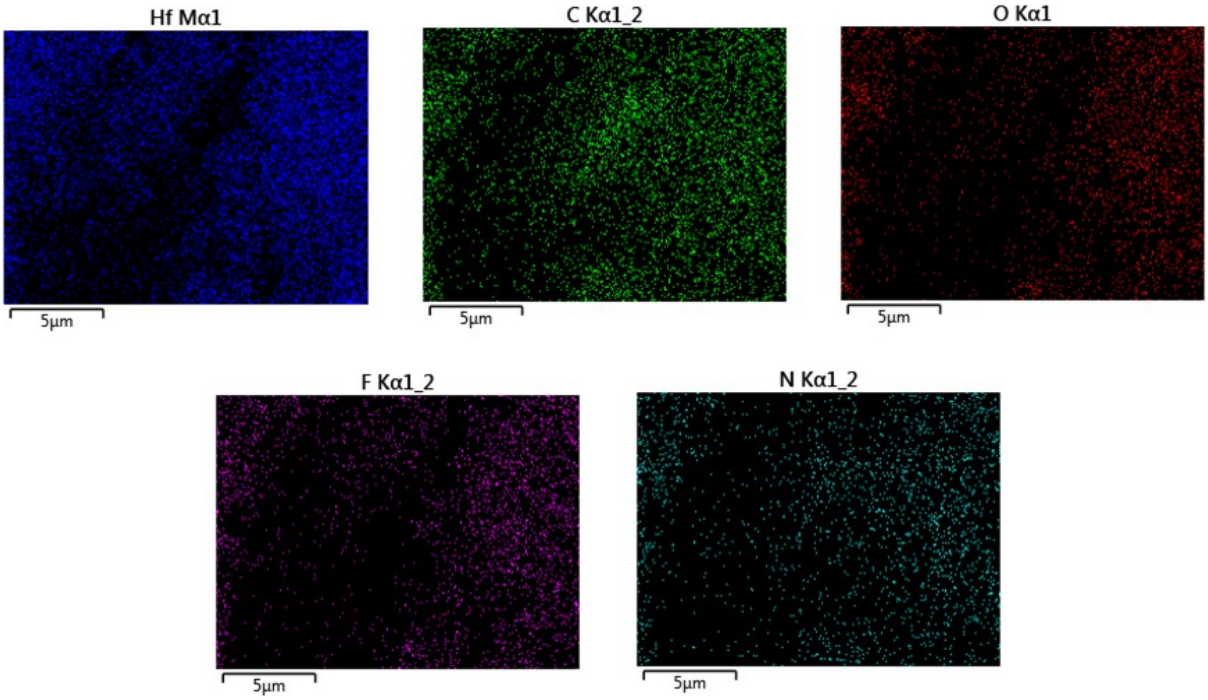

Fig. S8. EDX elemental mapping of **1′**.

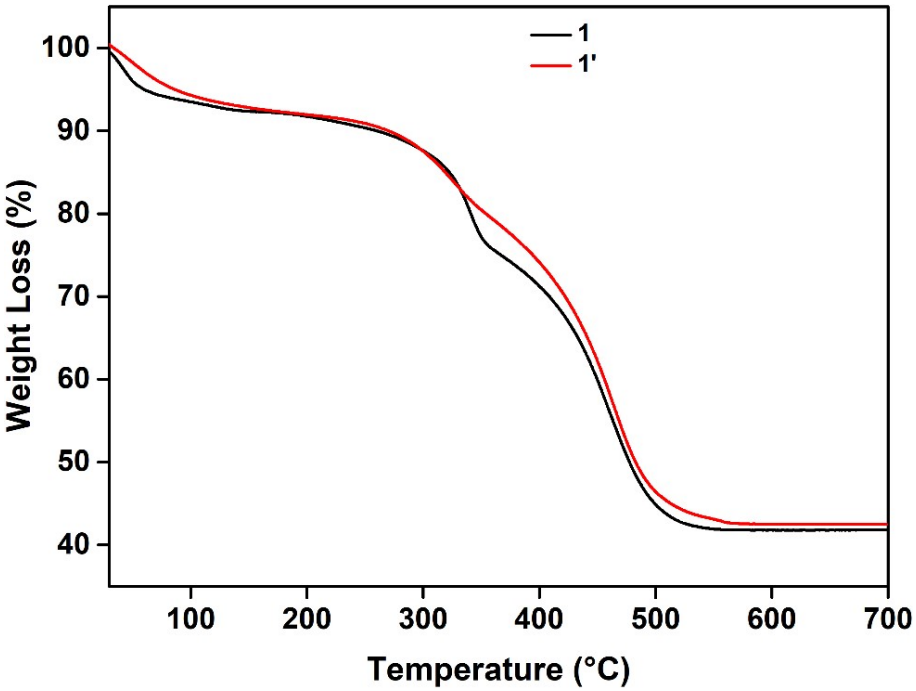

Fig. S9. Thermogravimetric analysis curves of as-synthesized **1** (black) and thermally activated **1′** (red) recorded under N_2 atmosphere in the temperature range of 30-700 °C with a heating rate of 4 °C min^{-1}.

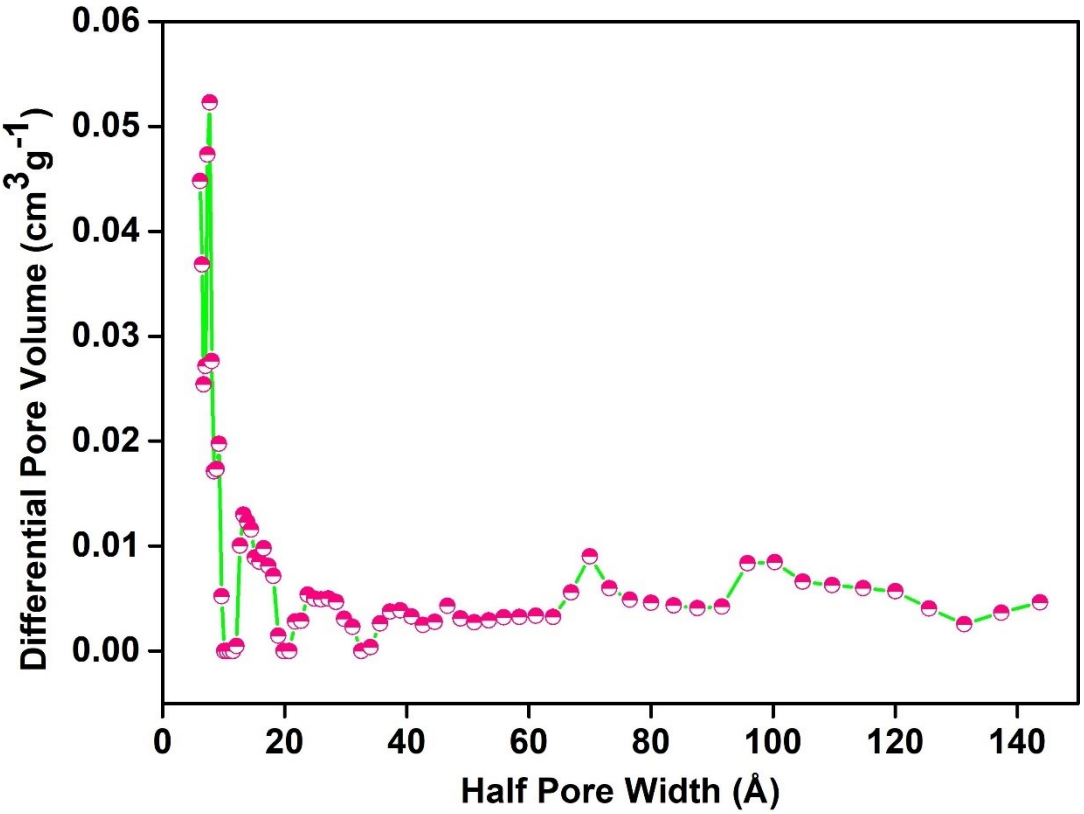

Fig. S10. Density functional theory pore-size distribution of compound **1′** as determined from its N_2 adsorption isotherms at -196 °C.

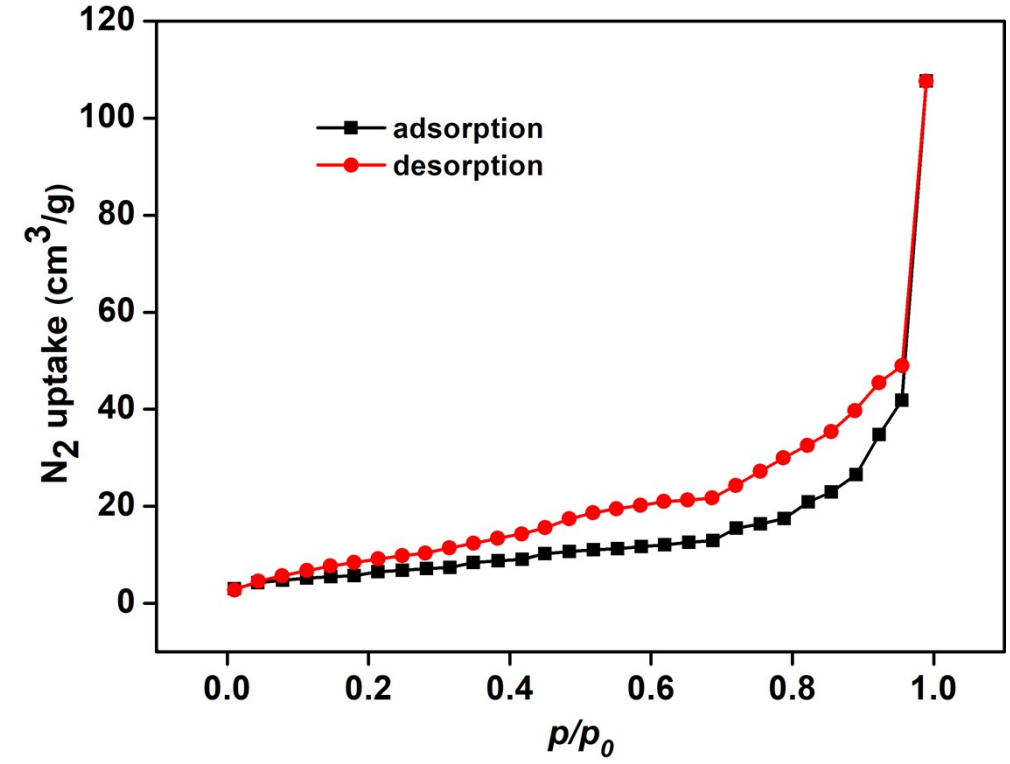

Fig. S11. N_2 adsorption (black squares) and desorption (red circles) isotherms of thermally activated **1** recorded at –196 °C.

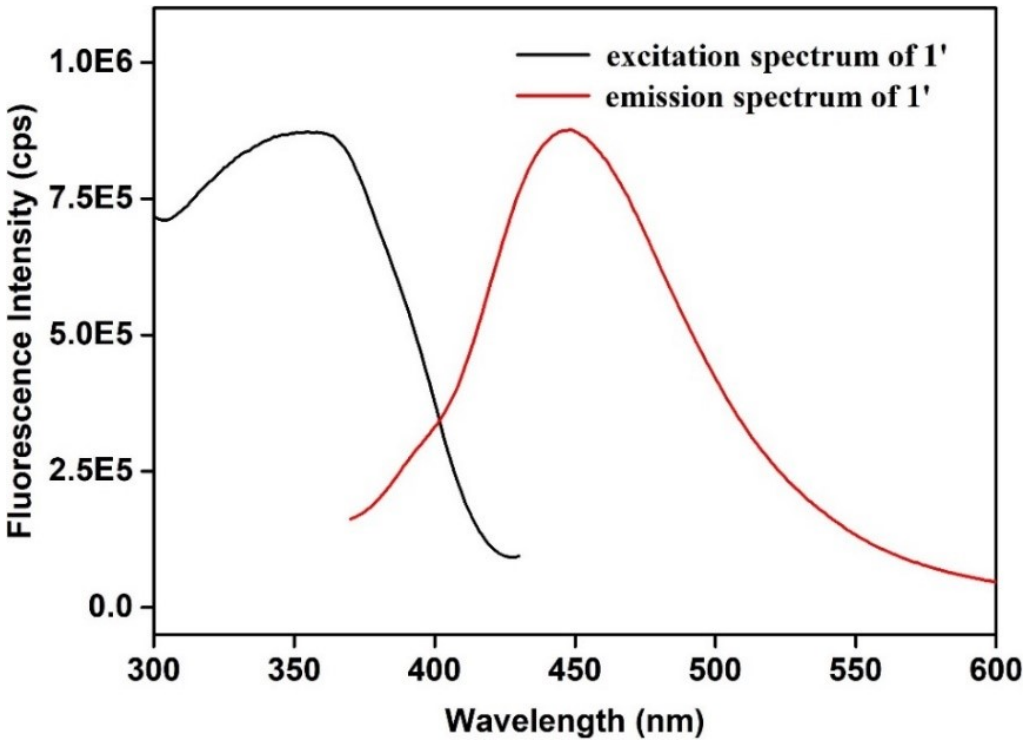

Fig. S12. Excitation (black) and emission (red) spectra of **1′** in water.

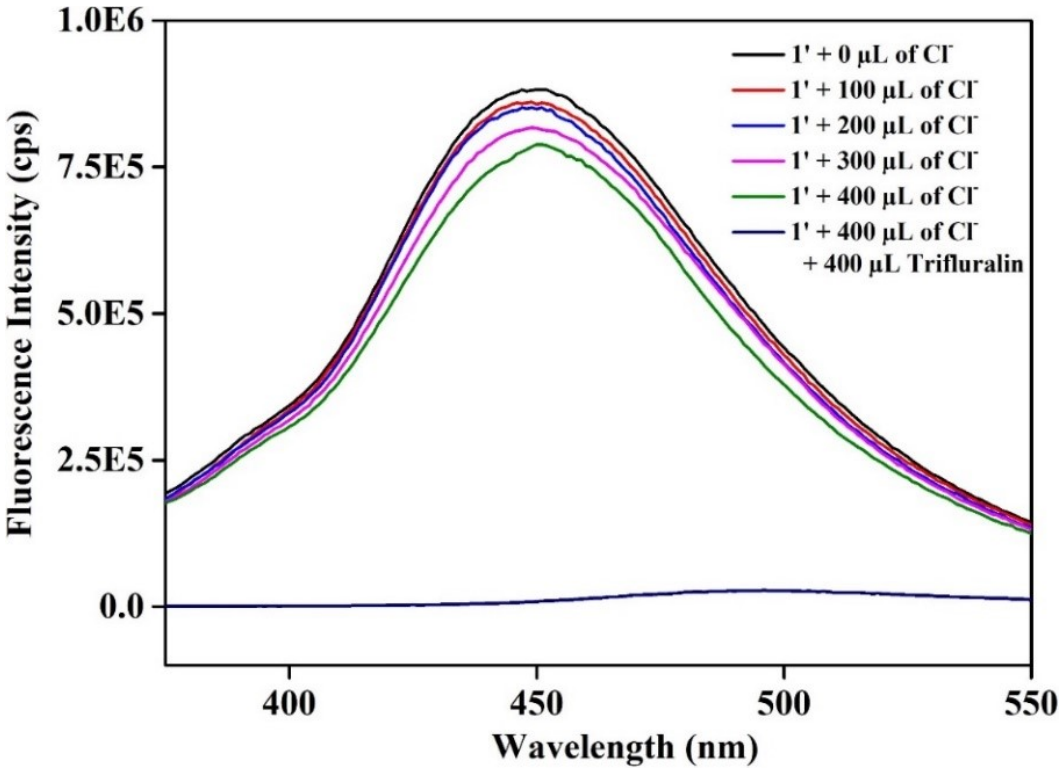

Fig. S13. Quenching in fluorescence emission intensity of the suspension of **1′** after addition of 400 µL of 10 mM trifluralin solution in presence of 400 µL of 10 mM solution of Cl^-.

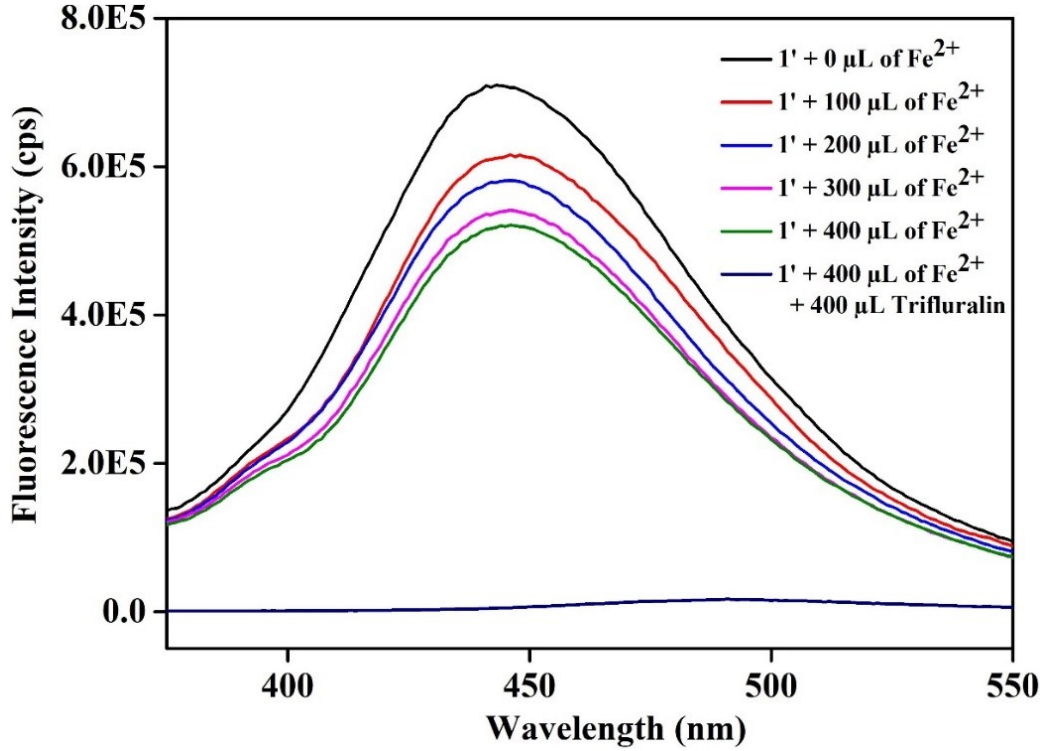

Fig. S14. Quenching in fluorescence emission intensity of the suspension of **1′** after addition of 400 µL of 10 mM trifluralin solution in presence of 400 µL of 10 mM solution of Fe^{2+}.

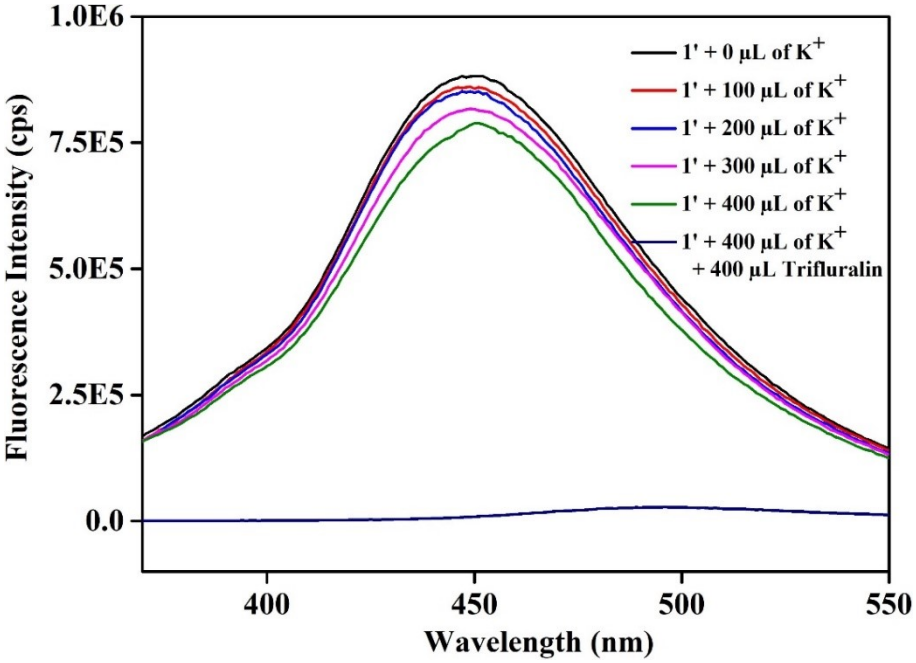

Fig. S15. Quenching in fluorescence emission intensity of the suspension of **1′** after addition of 400 µL of 10 mM trifluralin solution in presence of 400 µL of 10 mM solution of K^+.

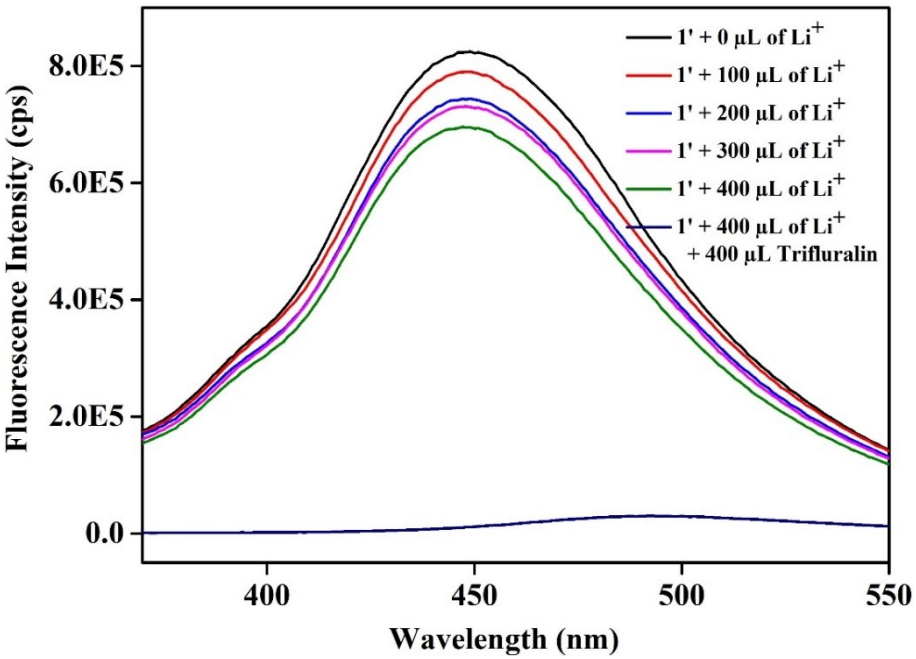

Fig. S16. Quenching in fluorescence emission intensity of the suspension of **1′** after addition of 400 µL of 10 mM aqueous trifluralin solution in presence of 400 µL of 10 mM solution of Li^+.

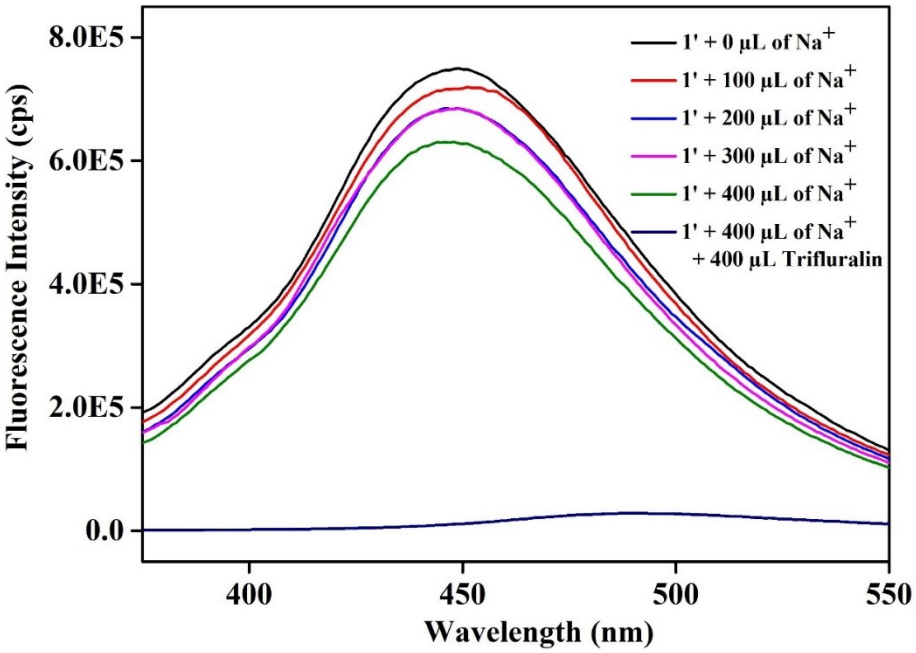

Fig. S17. Quenching in fluorescence emission intensity of the suspension of **1′** after addition of 400 µL of 10 mM trifluralin solution in presence of 400 µL of 10 mM solution of Na^+.

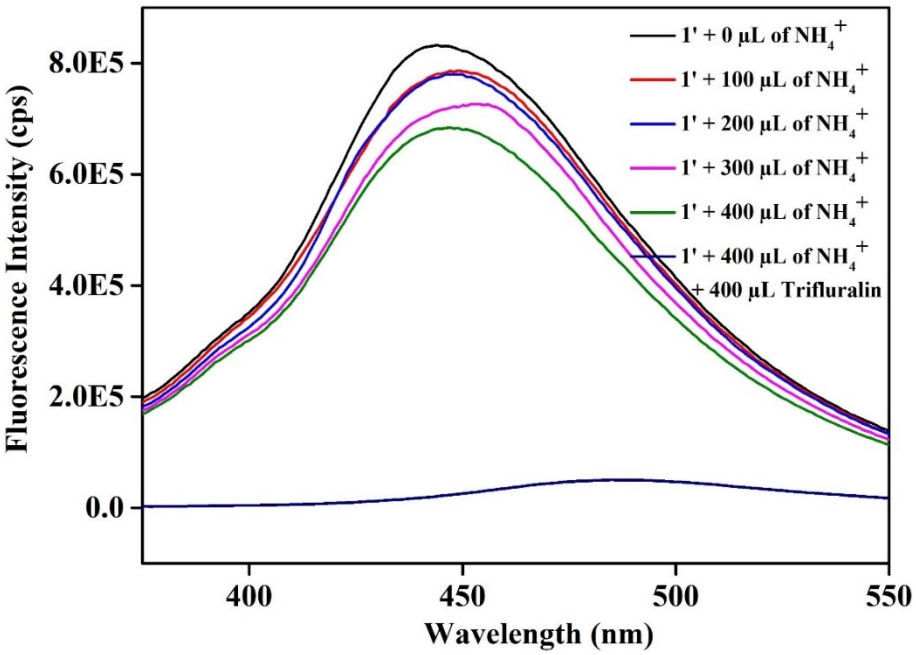

Fig. S18. Quenching in fluorescence emission intensity of the suspension of **1′** after addition of 400 µL of 10 mM trifluralin solution in presence of 400 µL of 10 mM solution of NH_4^+.

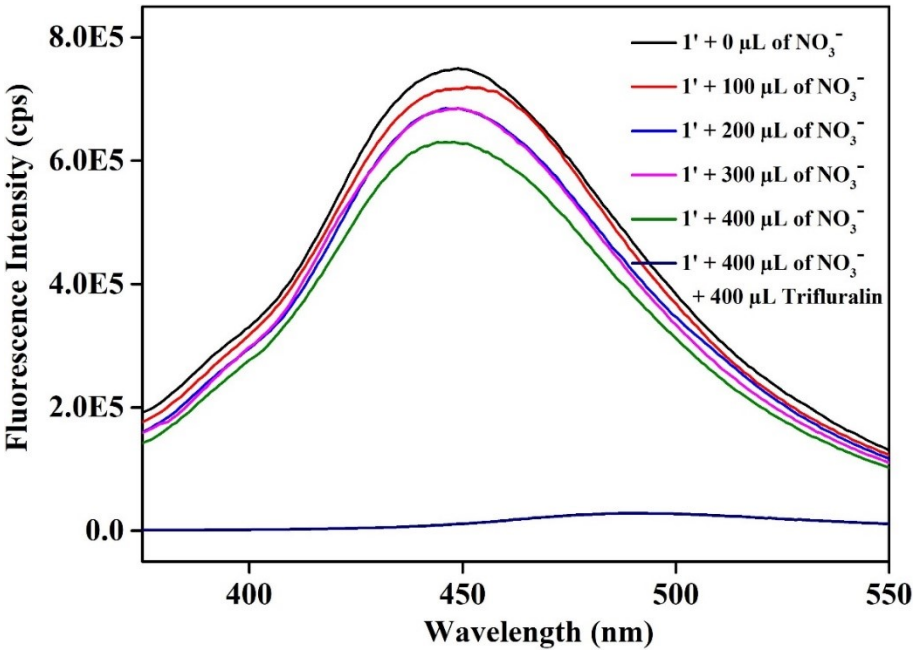

Fig. S19. Quenching in fluorescence emission intensity of the suspension of **1′** after addition of 400 µL of 10 mM trifluralin solution in presence of 400 µL of 10 mM solution of NO_3^-.

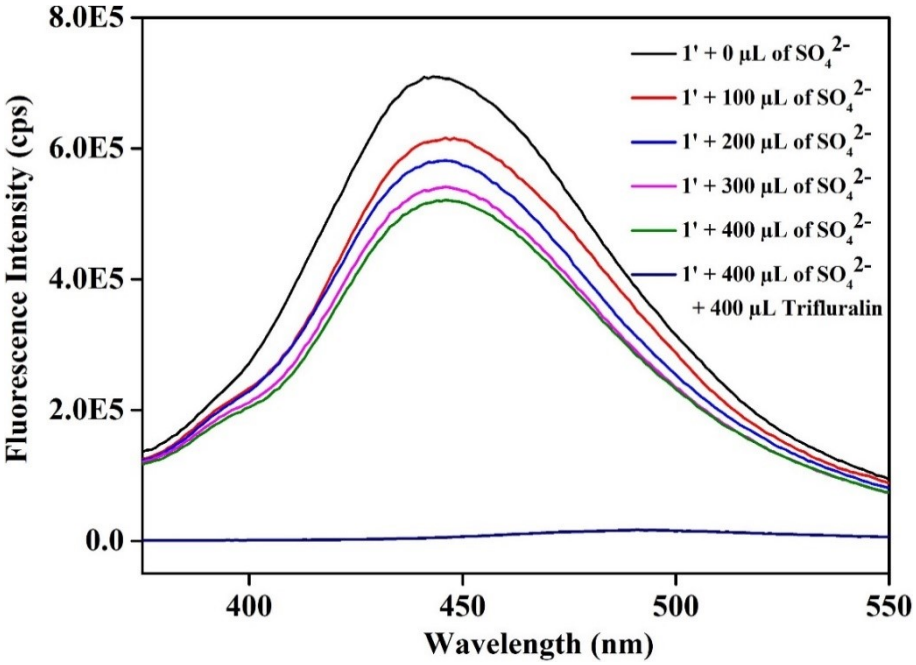

Fig. S20. Quenching in fluorescence emission intensity of the suspension of **1′** after addition of 400 µL of 10 mM aqueous trifluralin solution in presence of 400 µL of 10 mM solution of SO_4^{2-}.

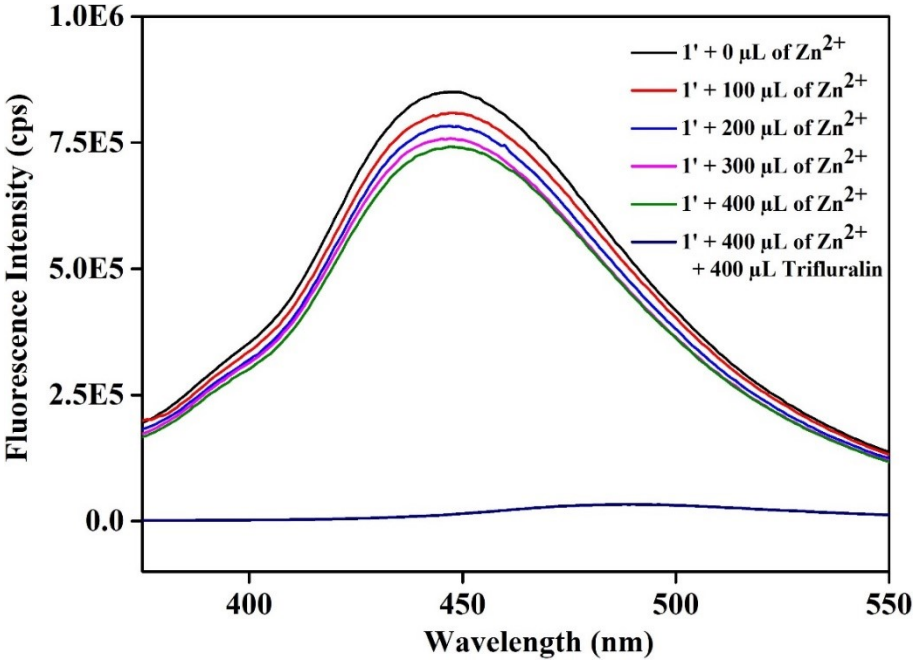

Fig. S21. Quenching in fluorescence emission intensity of the suspension of **1′** after addition of 400 µL of 10 mM aqueous trifluralin solution in presence of 400 µL of 10 mM solution of Zn^{2+}.

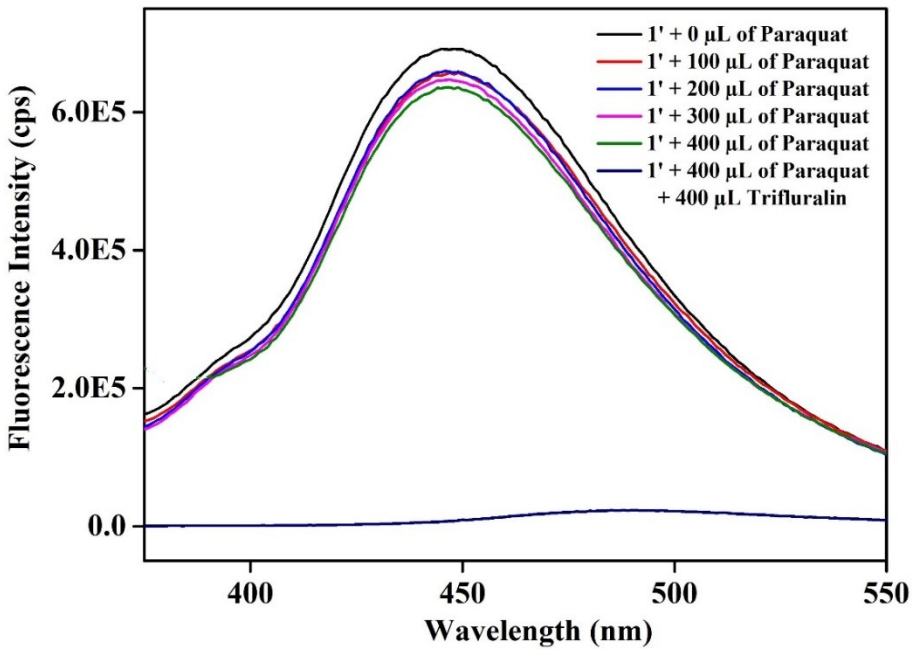

Fig. S22. Quenching in fluorescence emission intensity of the suspension of **1′** after addition of 400 µL of 10 mM trifluralin solution in presence of 400 µL of 10 mM solution of paraquat.

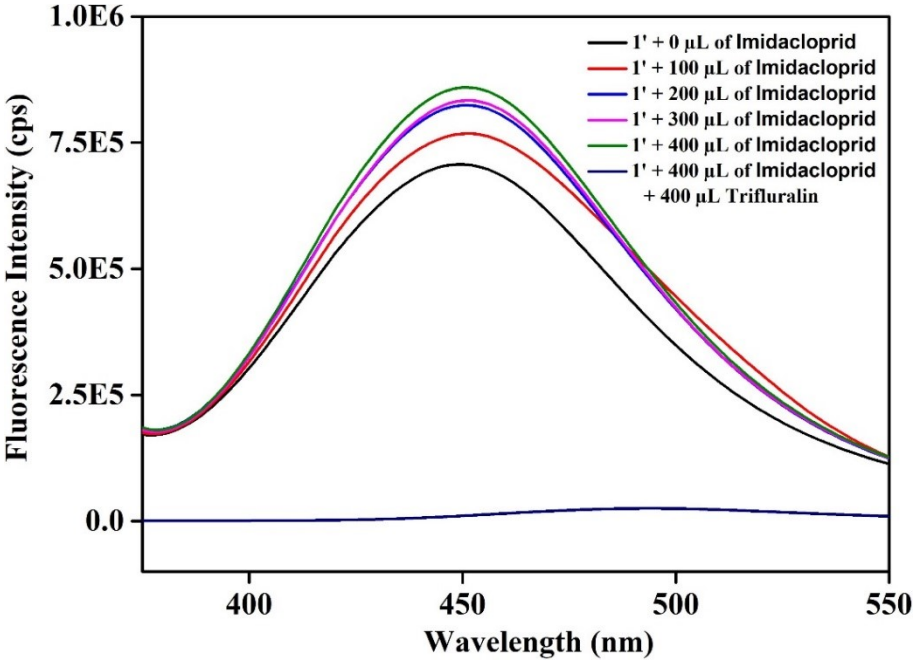

Fig. S23. Quenching in fluorescence emission intensity of the suspension of **1′** after addition of 400 µL of 10 mM trifluralin solution in presence of 400 µL of 10 mM solution of imidacioptid.

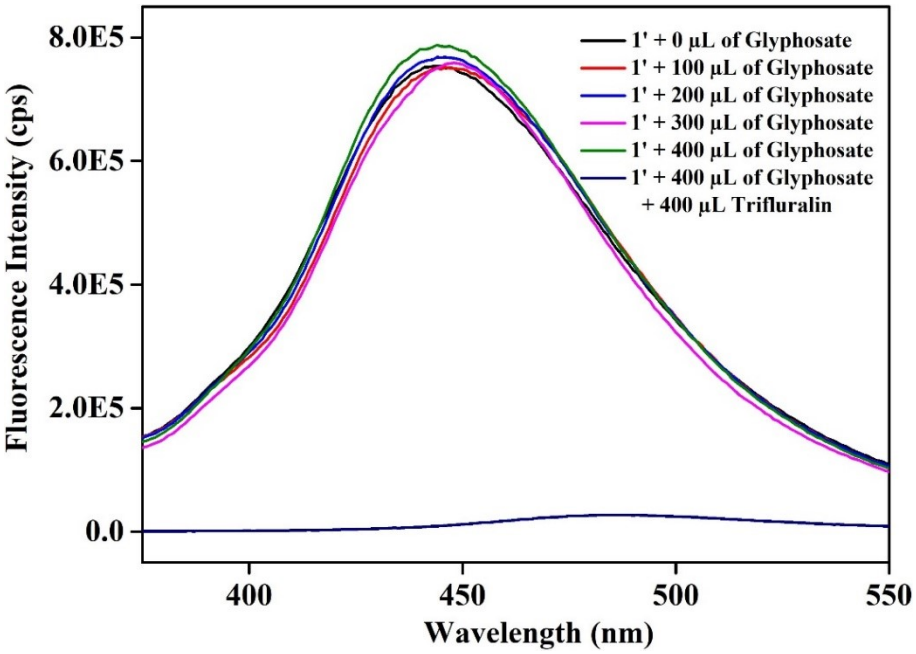

Fig. S24. Quenching in fluorescence emission intensity of the suspension of **1′** after addition of 400 µL of 10 mM trifluralin solution in presence of 400 µL of 10 mM solution of glyphosate.

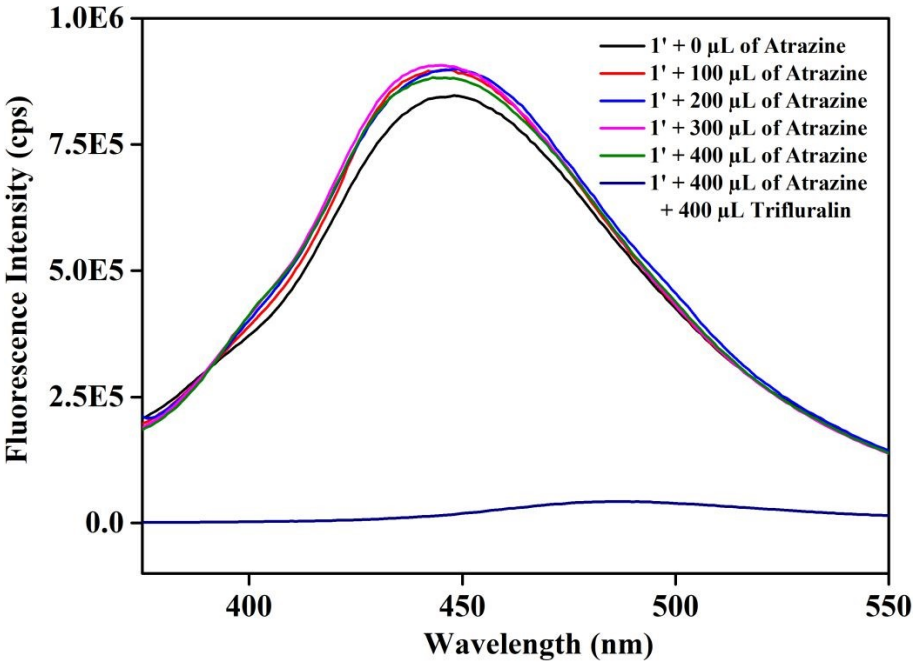

Fig. S25. Quenching in fluorescence emission intensity of the suspension of **1′** after addition of 400 µL of 10 mM trifluralin solution in presence of 400 µL of 10 mM solution of atrazine.

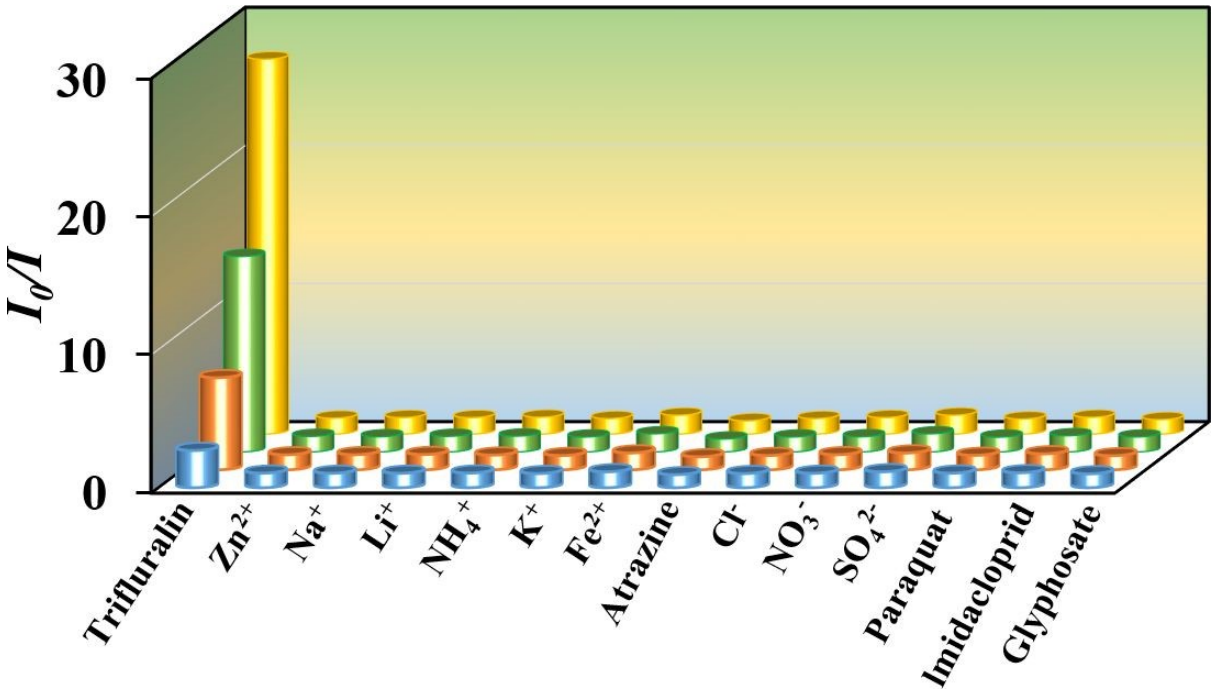

Fig. S26. Stern-Volmers plot for the decrease in luminescence intensities of **1′** with gradual addition of various analytes in case of trifluralin sensing.

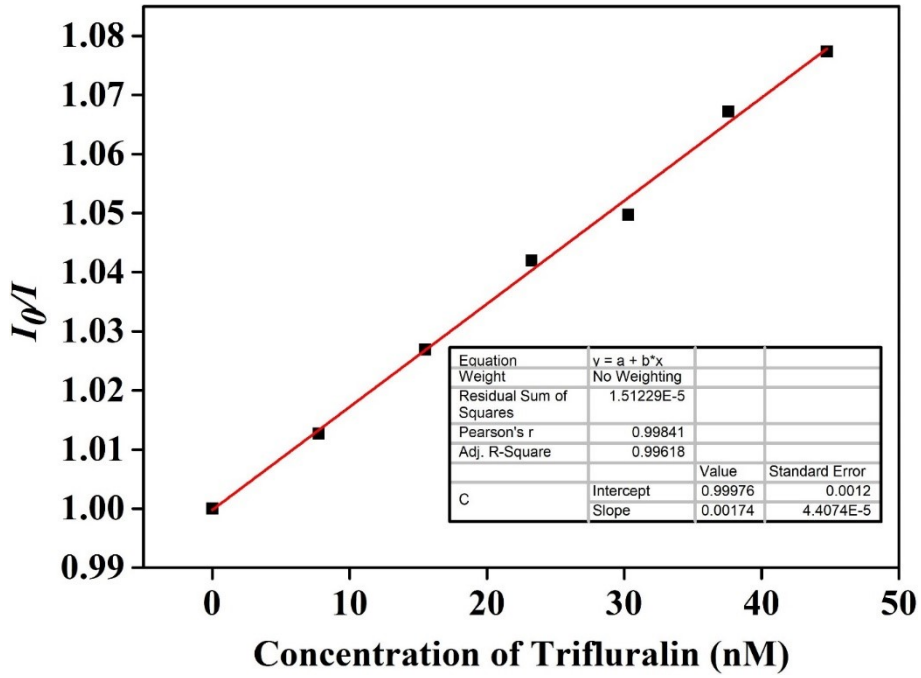

Fig. S27. Stern-Volmer plot for the fluorescence emission quenching of **1′** in presence of trifluralin.

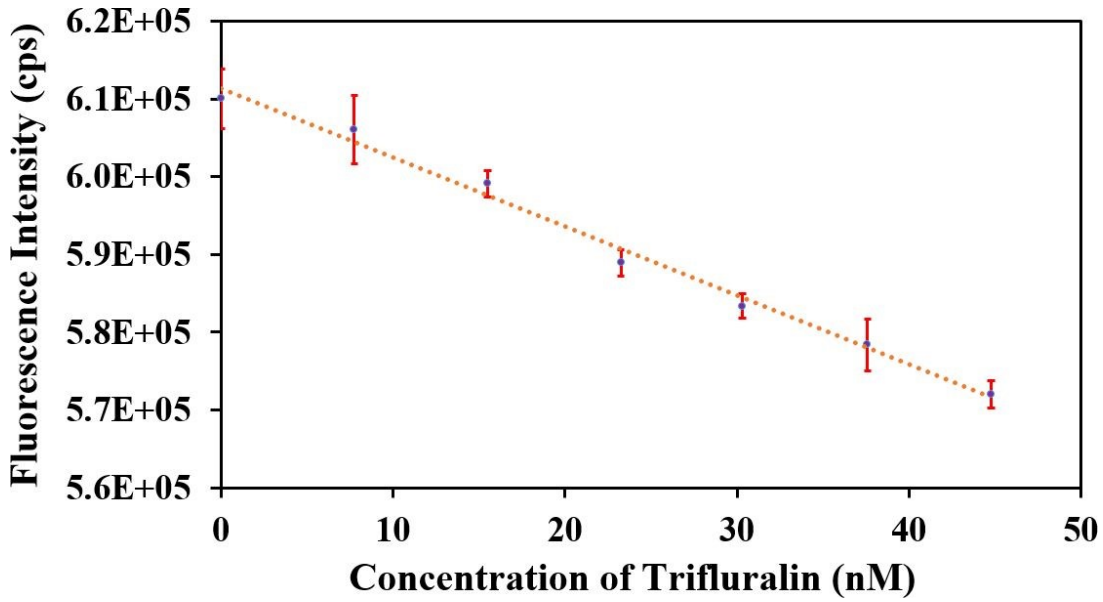

Fig. S28. Change in the fluorescence emission intensity of **1′** as a function of concentration of trifluralin.

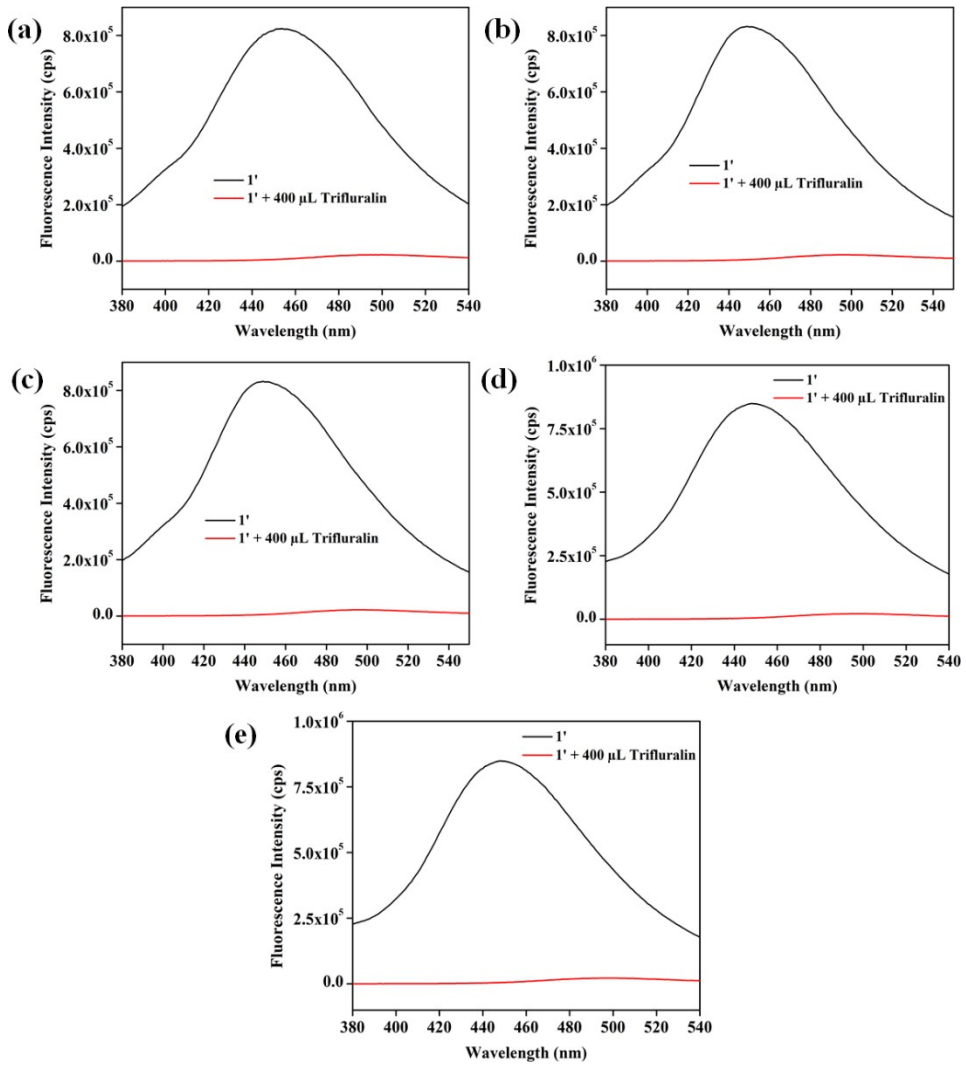

Fig. S29. Change in the fluorescence emission intensity of **1′** after (a) 1st , (b) 2nd, (c) 3rd (d) 4th and (e) 5th cycle of trifluralin sensing.

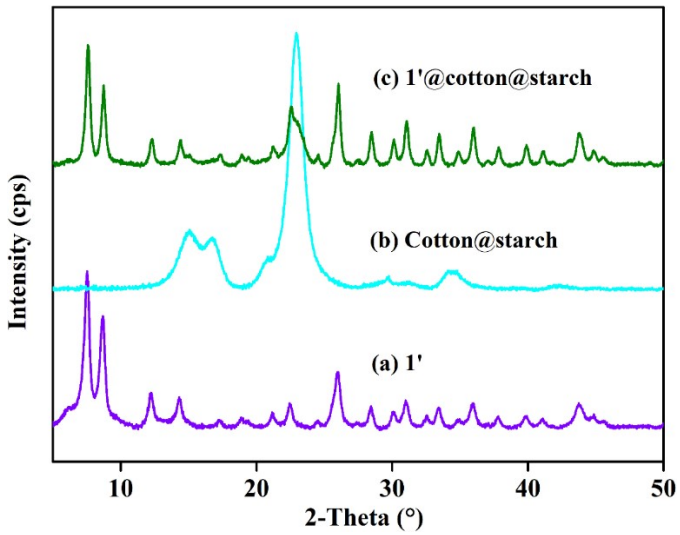

Fig. S30. PXRD patterns of (a) **1′**, (b) cotton@starch and (c) **1′**@cotton@starch composite.

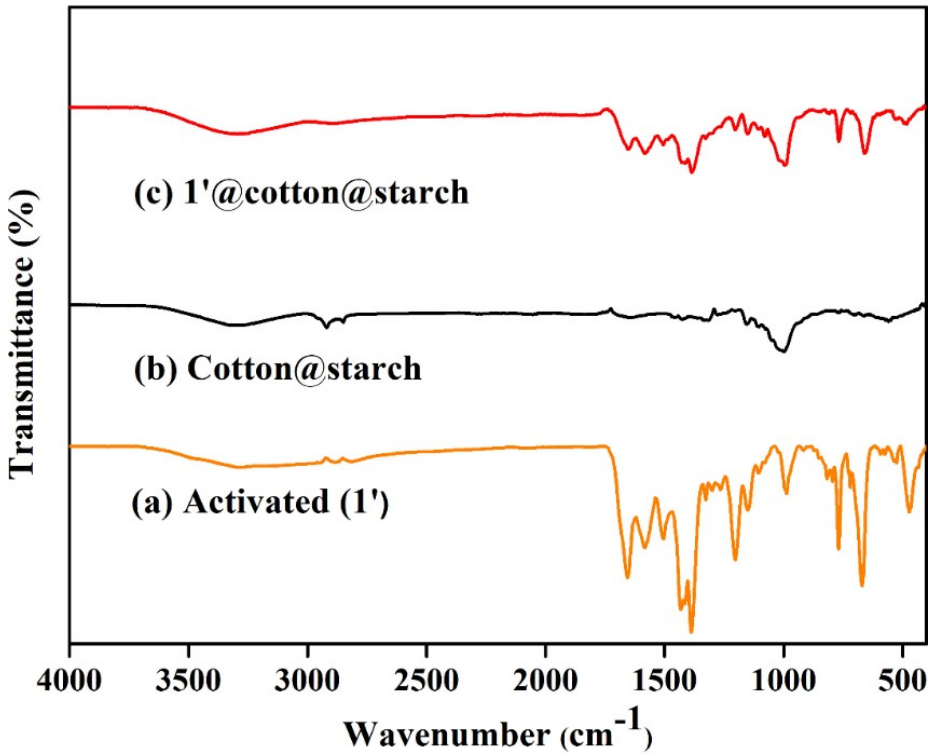

Fig. S31. ATR-IR spectra of compound (a) **1′**, (b) cotton@starch and (c) **1′**@cotton@starch composite.

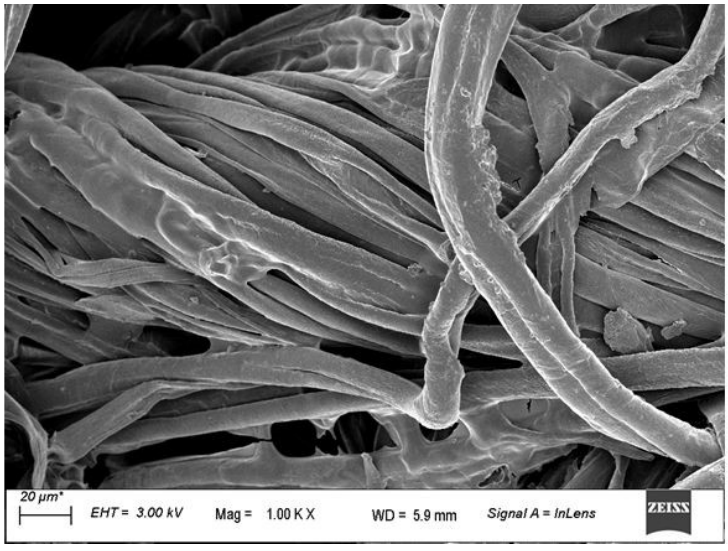

Fig. S32. FE-SEM images of (a) cotton@starch and (b) **1′**@cotton@starch composite.

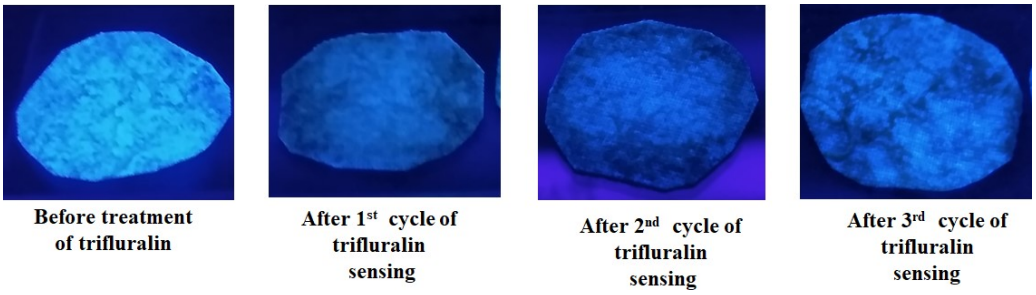

Fig. S33. Digital images of **1′**@cotton@chitosan composite after each cycle of sensing of trifluralin.

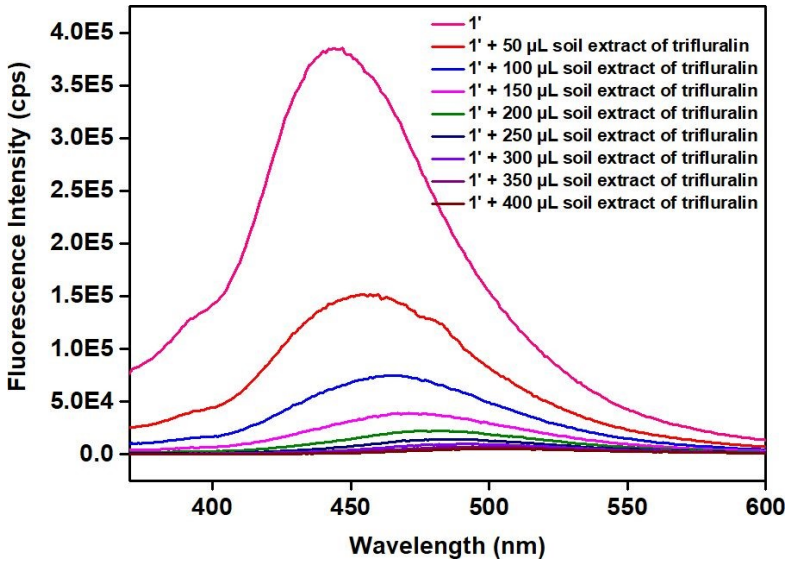

Fig. S34. Change in fluorescence intensity of **1′** after the addition of different volumes of trifluralin-spiked soil extracts.

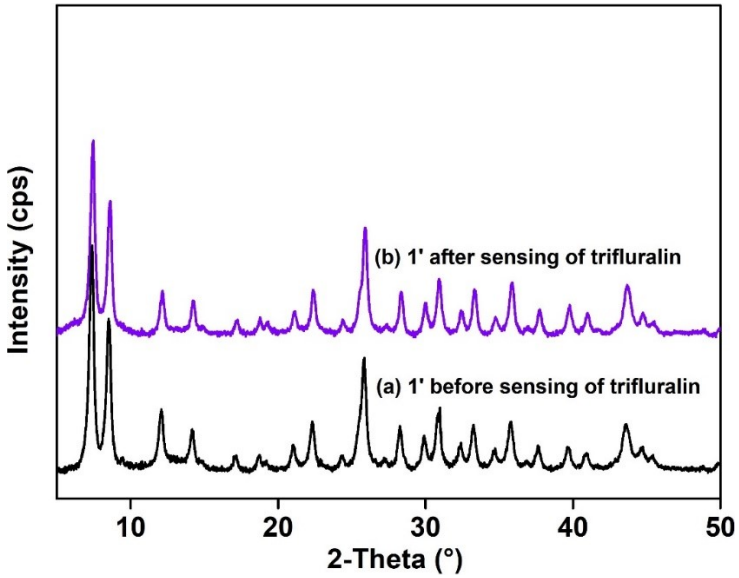

Fig. S35. PXRD patterns of **1′** before (a) and after treatment with trifluralin.

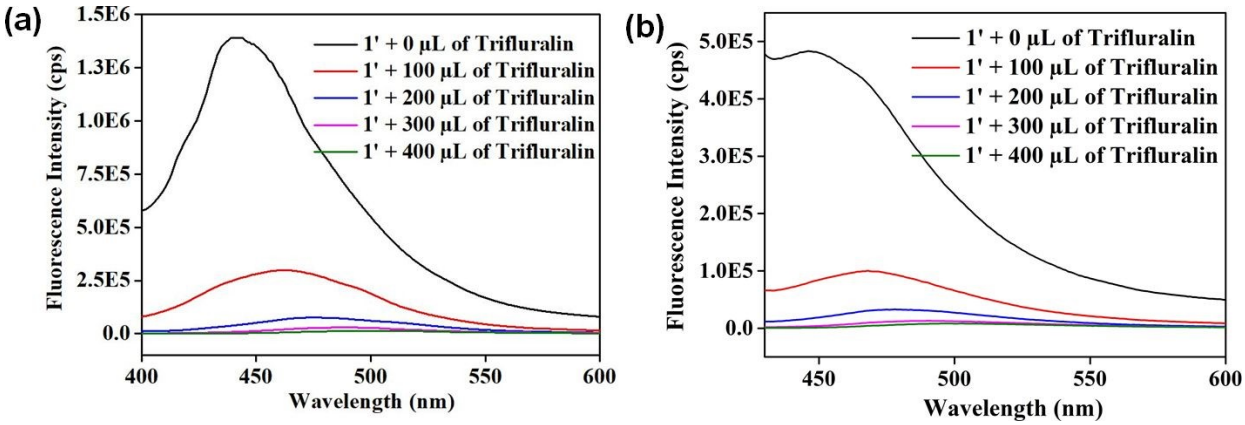

Fig. S36. Sensing of trifluralin after excitation of **1′** suspension at (a) 380 nm and (b) 410 nm.

Table S2. Fluorescence lifetimes of **1′** before and after the addition of trifluralin solution (λ_{ex} = 374 nm, pulsed diode laser).

Volume of trifluralin Solution Added (µL)	a_1	a_2	a_3	τ_1 (ns)	τ_2 (ns)	τ_3 (ns)	$<\tau>$* (ns)	χ^2
0	0.40	0.44	0.17	1.09	7.75	0.05	3.85	1.14
400	0.39	0.50	0.11	0.83	2.85	0.05	1.75	1.07

* $<\tau> = a_1\tau_1 + a_2\tau_2$

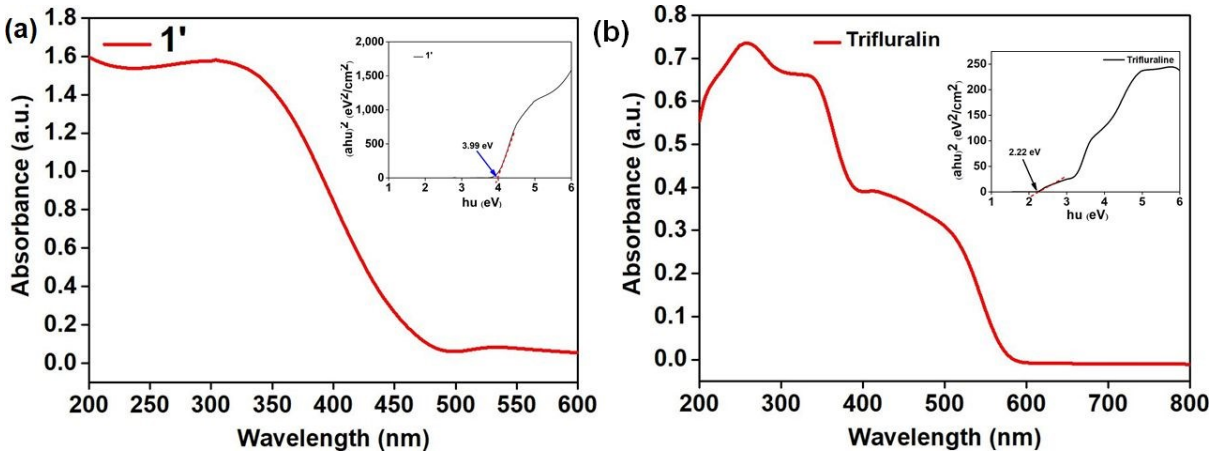

Fig. S37. (a) UV-DRS spectra of **1′** and (b) trifluralin (Tauc plots are shown inset).

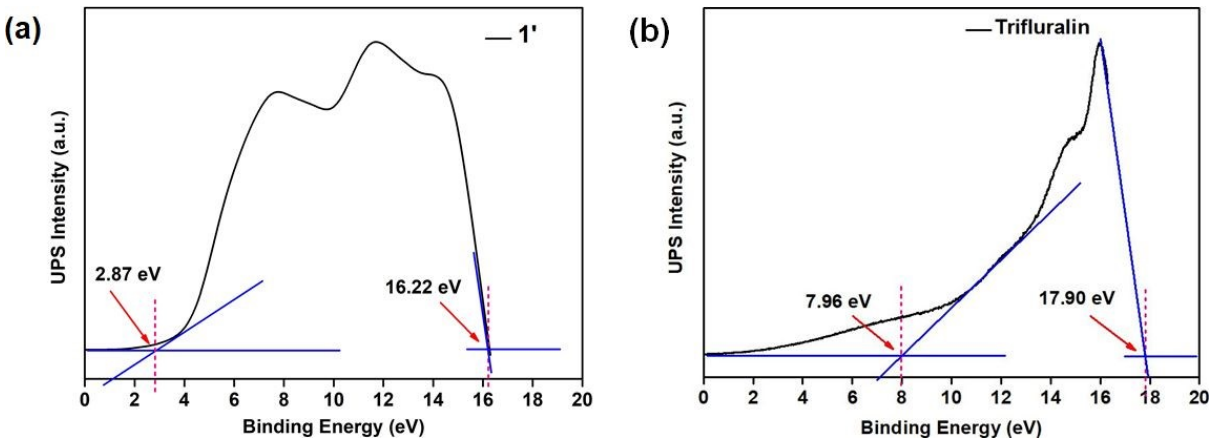

Fig. S38. (a) UPS spectrum of **1′** and (b) trifluralin.

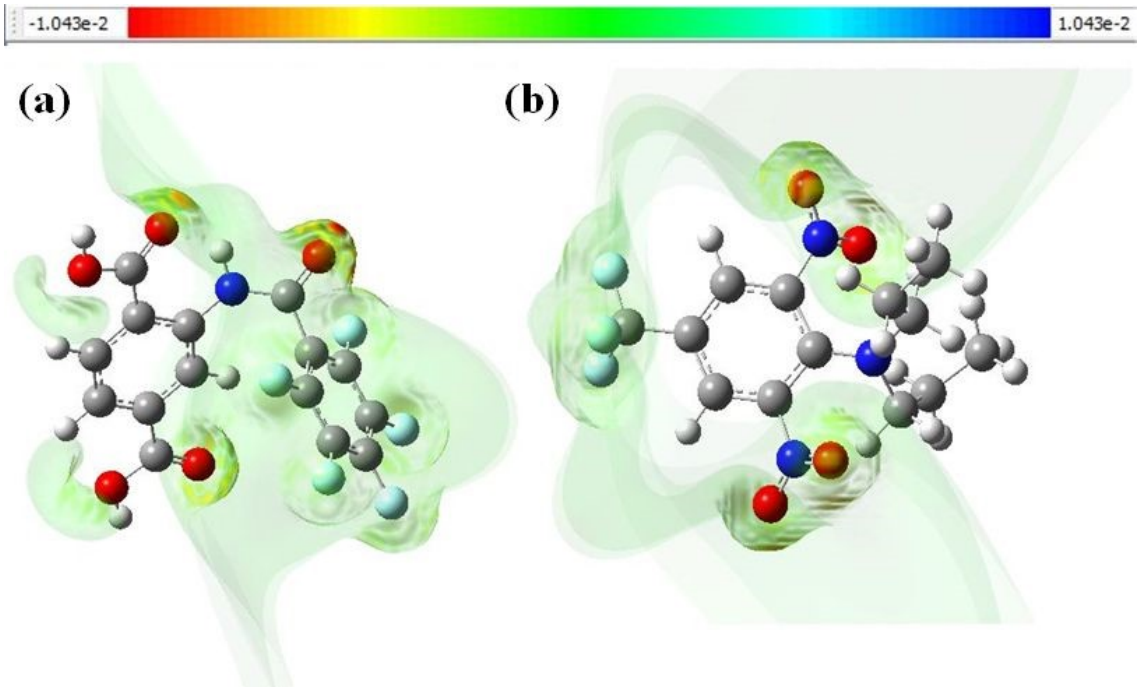

Fig. S39. ESP surfaces of (a) H_2L linker and (b) trifluralin.

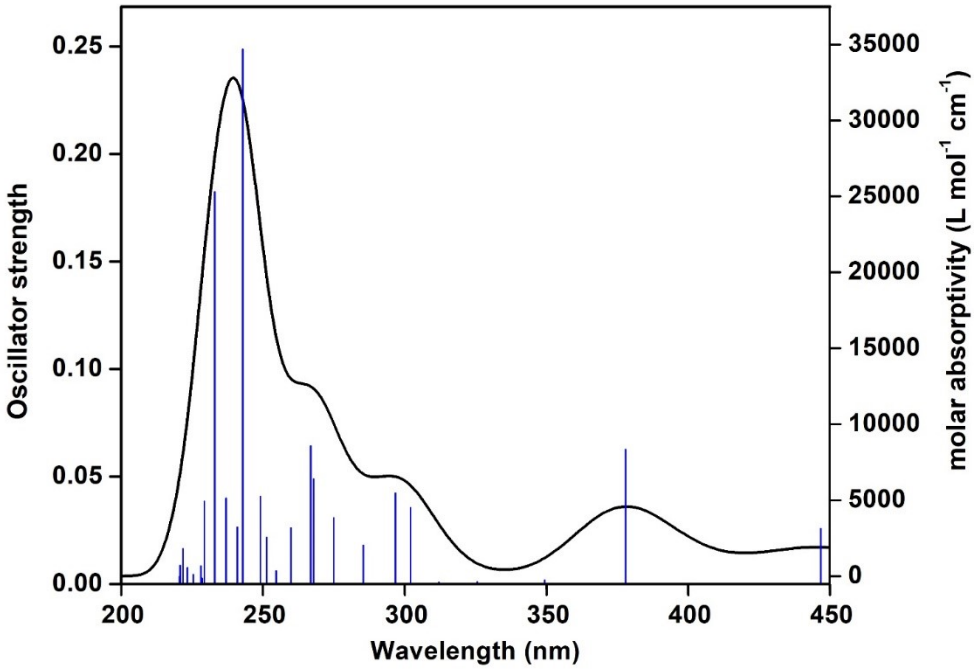

Fig. S40. Computationally predicted UV-Vis spectrum of H_2L liker in the gas phase. Blue lines indicate the main singlet electronic transitions.

Table S3. Statistical details of different analytical parameters for the sensing of trifluralin by **1′**.

Concentration Range (nM)	Slopes	Intercepts	Correlation Coefficient (R^2)	$S_{y/x}$ [a]	LOD[b] (nM)	LOQ[c] (nM)	Regression Equation
0-44.8	895.9	612364.1	0.998	4957.7	16.6	55.3	895.9x + 612364.1
	919.2	612421.8	0.995	4646.2	15.2	50.5	919.2x + 612421.8
	846.6	609118	0.997	4872.3	17.2	57.5	846.6x + 609118
Average	887.2	611301.7	0.996	4825.4	16.3	54.5	887.2x + 611301.7
SD	37.09	1891.3	0.002	160.9	1.07	3.58	(887.2 ± 37.09)x + (611301.7 ± 1891.3)

[a] Standard deviation of the residuals, [b] Limit of detection, [c] Limit of quantification

Table S4. Comparison between the spiked and observed concentrations and recovery of trifluralin in different real water specimens.

Type of Water	Spiked Conc. of Trifluralin (μM)	Observed Conc. of Trifluralin (μM)	Recovery (%)
Milli-Q Water	(i) 1111.1 (ii) 555.5 (iii) 277.7	(i) 1105.0 (ii) 540.4 (iii) 268.5	(i) 99.4 (ii) 97.3 (iii) 96.7
Lake Water	(i) 1111.1 (ii) 555.5 (iii) 277.7	(i) 1102.9 (ii) 552.5 (iii) 264.1	(i) 99.3 (ii) 99.4 (iii) 95.1
Tap Water	(i) 1111.1 (ii) 555.5 (iii) 277.7	(i) 1100.2 (ii) 545.1 (iii) 270.6	(i) 99.0 (ii) 98.1 (iii) 97.4
River Water	(i) 1111.1 (ii) 555.5 (iii) 277.7	(i) 1106.2 (ii) 541.2 (iii) 270.7	(i) 99.5 (ii) 97.4 (iii) 97.4

Table S5. Evaluation of intra-day, inter-day accuracy and precision study of change in fluorescence intensity of **1′** after incremental addition of 10 mM aqueous solution of trifluralin.

Parameter	Amount of Trifluralin Added (μL)	Fluorescence Intensity (cps) at λ_{max} = 448 nm			Average PL Intensity (cps)	SD	RE%
Repeatability Intra-day precision	0	875895.7	872416.6	871198.7	873170.4	2437.5	0.003
	100	304303.2	306444.6	310159.6	306969.1	2963.2	0.008
	200	94076.2	96570.1	98386.4	96344.2	2163.9	0.023
	300	33241.6	34548.1	35478.2	34422.6	1123.6	0.034
	400	11292.2	11834.4	12414.2	11846.9	561.1	0.047
Reproducibility Inter-day precision	0	875895.7	867234.5	863843.2	868991.2	6215.3	0.101
	100	304303.2	312394.8	314458.8	310385.6	5367.6	0.073
	200	94076.2	101172.1	103088.2	99445.5	4747.5	0.054
	300	33241.6	36448.5	3786.4	35850.8	2367.7	0.019
	400	11292.2	12958.5	13447.5	12566.1	1129.9	0.007

Table S6. TDDFT vertical gas phase energies of the lowest lying singlet state for H_2L linker.

Transition No.	Wavelength (nm)	Oscillator Strength (*f*)	Major contribution
2	377.9	0.063	HOMO → L+1 (90%)
6	302.0	0.036	H-2 → LUMO (84%)
7	296.8	0.042	H-3 → LUMO (25%), H-1 → L+1 (41%)
10	274.9	0.031	H-4 → LUMO (73%)
11	267.9	0.049	H-5 → LUMO (34%), H-2 → L+1 (34%)
12	266.8	0.064	H-5 → LUMO (25%), H-2 → L+1 (42%)
14	259.8	0.026	HOMO → L+4 (49%) HOMO → L+5 (27%)
15	254.6	0.006	H-6 → LUMO (22%), H-4 → L+1 (59%)
16	251.3	0.022	H-1 → L+2 (33%),
17	249.1	0.041	H-6 → LUMO (27%), H-1 → L+2 (44%)
18	242.8	0.249	HOMO → L+5 (27%)
19	240.9	0.026	H-6 → L+1 (60%)
20	237.0	0.040	H-7 → LUMO (40%)
21	232.9	0.182	H-2 → L+2 (62%)
22	229.2	0.038	H-1 → L+3 (82%)

[a] Oscillator strength (*f*) > 0.02 are listed in the table.

[b] Contribution>20% are listed in the table.

Table S7. Comparison of the detection performance of present probe (**1′**) with some previously reported fluorescent probes of trifluralin.

Sl. No.	Sensor Material	Type of Material	Sensing Medium	Detection Limit	Response Time	Ref.
1	Imidazoles fluorescent probe	Organic molecule	THF/MeOH	5.066 μM	-	3
2	**$[Hf_6O_4(OH)_4(C_{15}H_4NO_5F_5)_6]$ (1′)**	**MOF**	**Water**	**16.3 nM**	**5 s**	**this work**

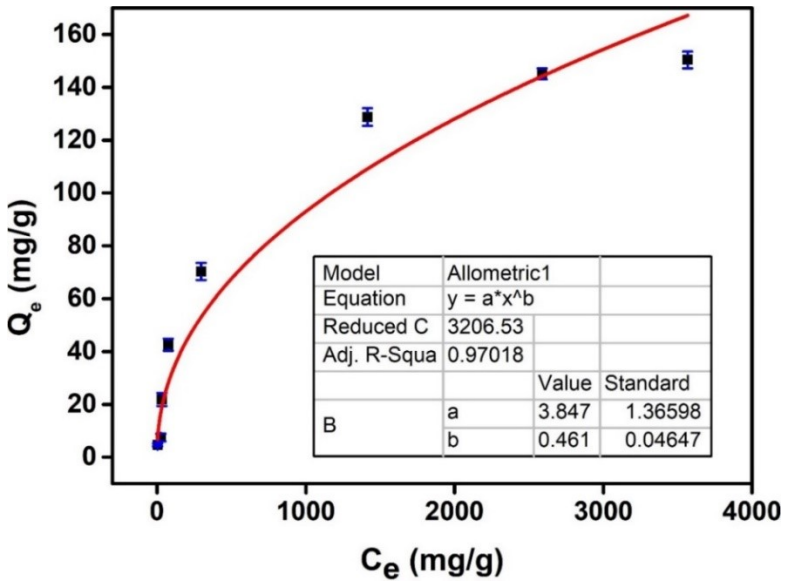

Fig. S41. Fitting of adsorption results of trifluralin on **1′** using the Freundlich model.

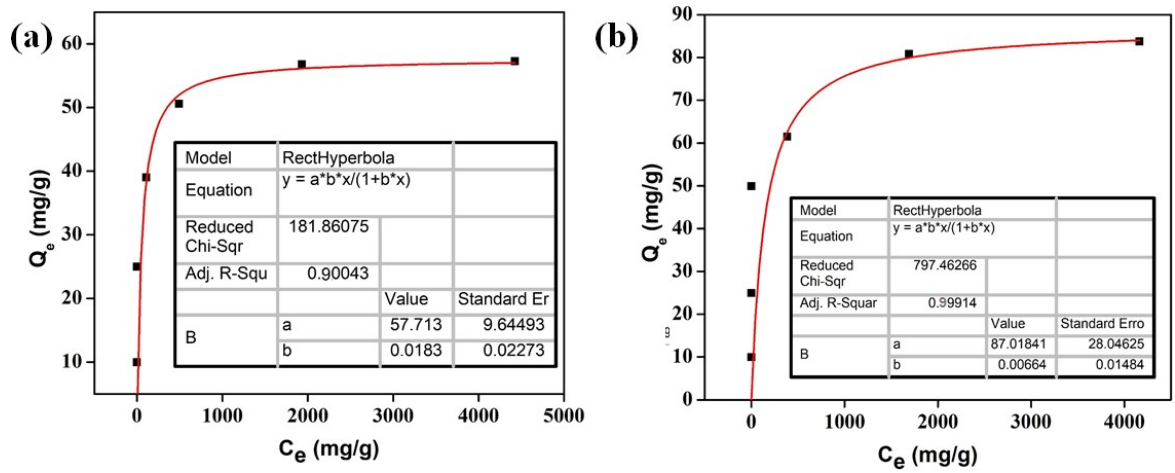

Fig. S42. Langmuir fitting of adsorption plot of trifluralin using the MOF formed with (a) 20 mmol and (b) 28 mmol trifluoroacetic acid at 150 °C as an adsorbent.

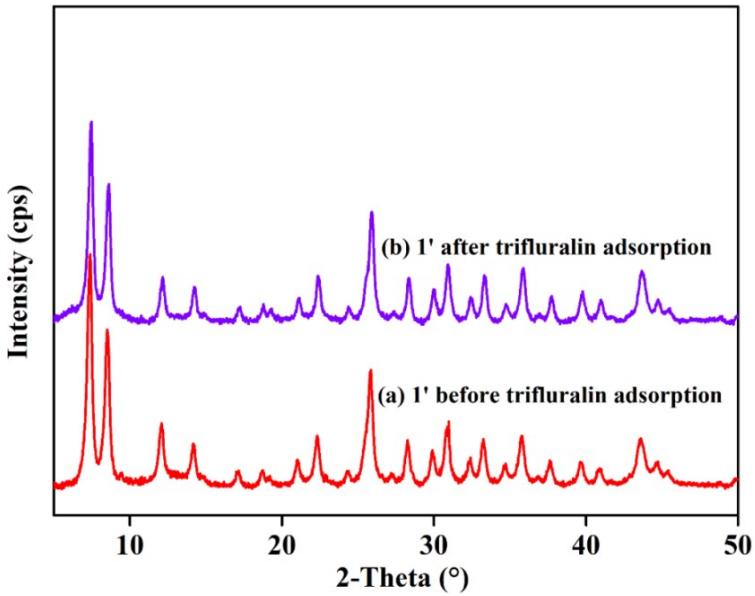

Fig. S43. PXRD patterns of **1′** before (a) and after trifluralin (b) adsorption.

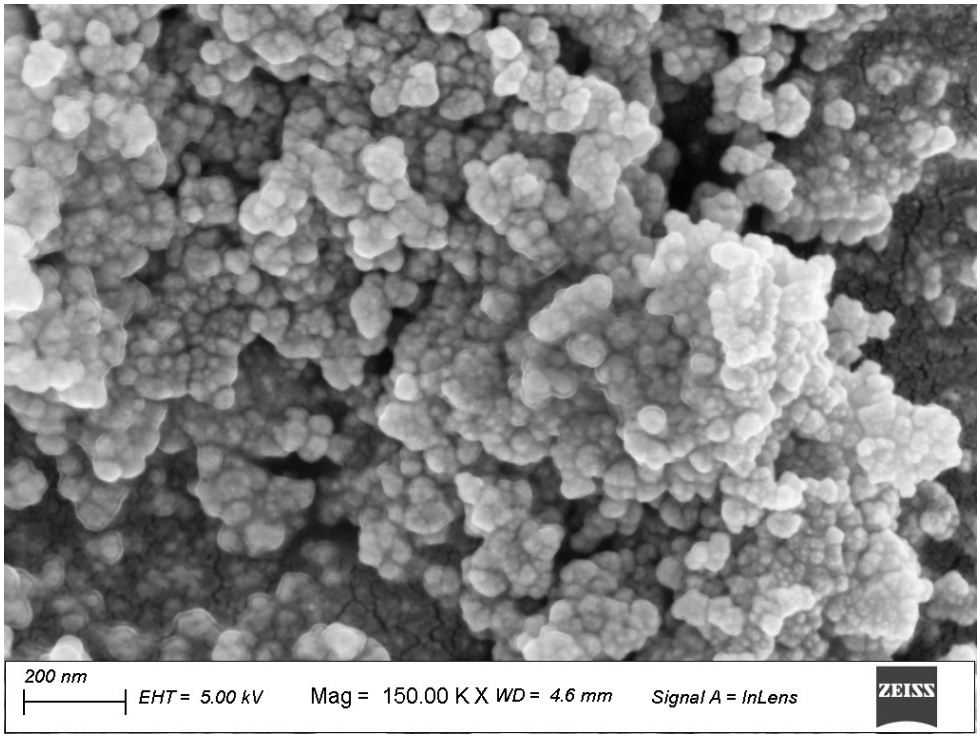

Fig. S44. FE-SEM images of **1′** after trifluralin adsorption experiment.

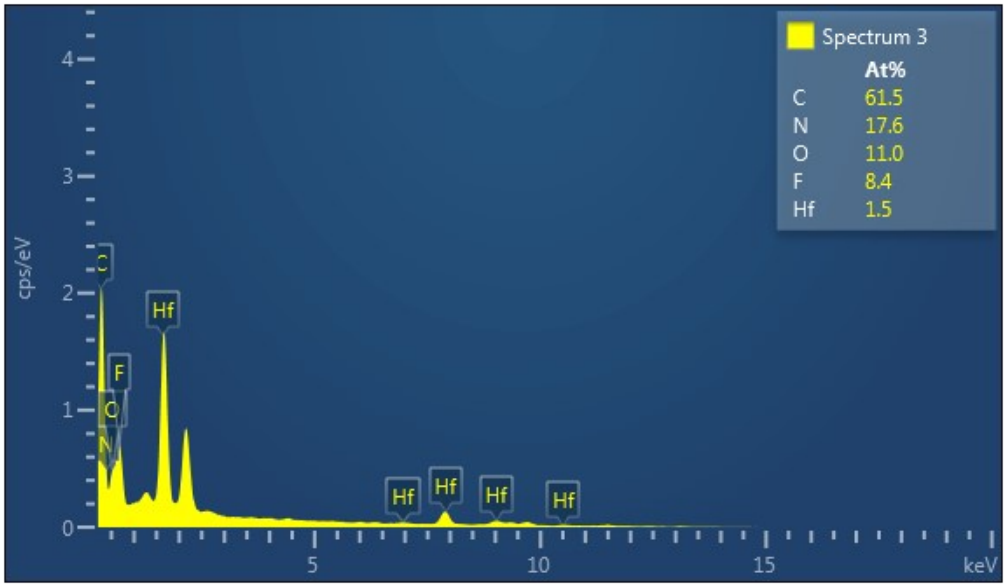

Fig. S45. EDX spectrum of **1′** after trifluralin adsorption experiment.

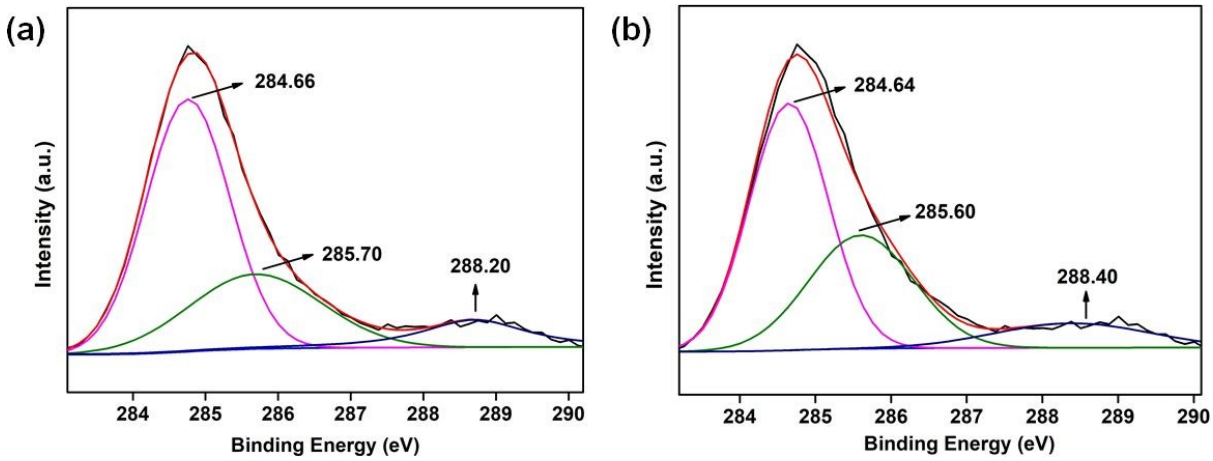

Fig. S46. Fitted XPS spectra of C (1s) of **1′** before (a) and after trifluralin (b) adsorption.

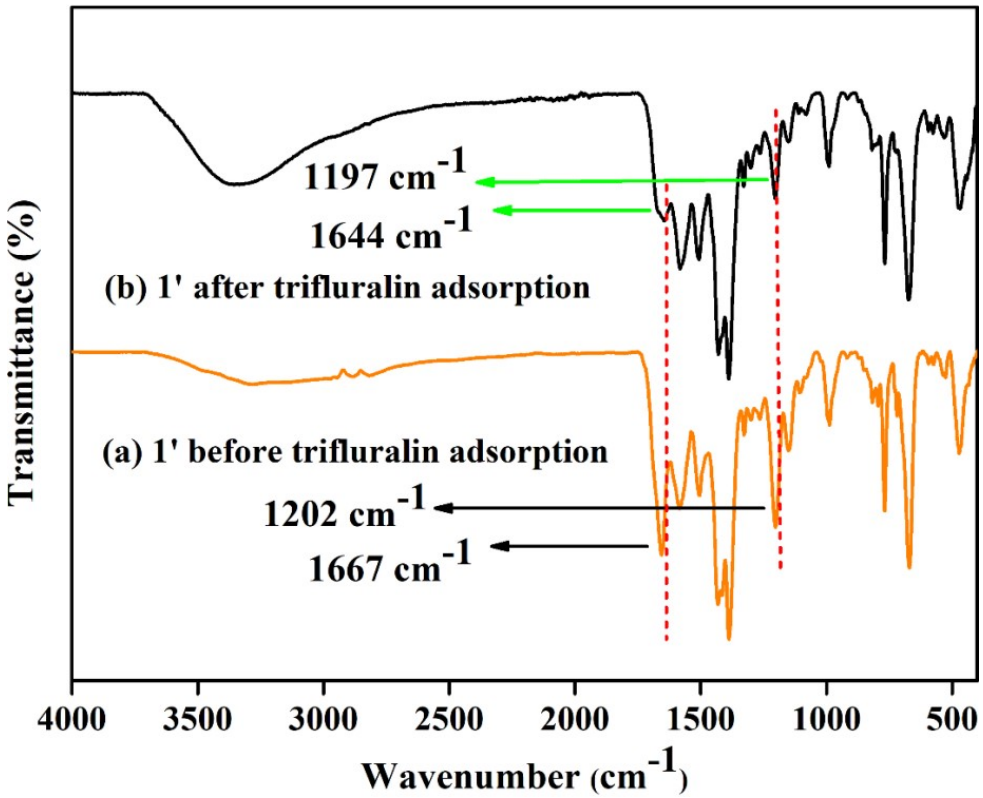

Fig. S47. ATR-IR spectra of **1′** before (a) and after trifluralin (b) adsorption.

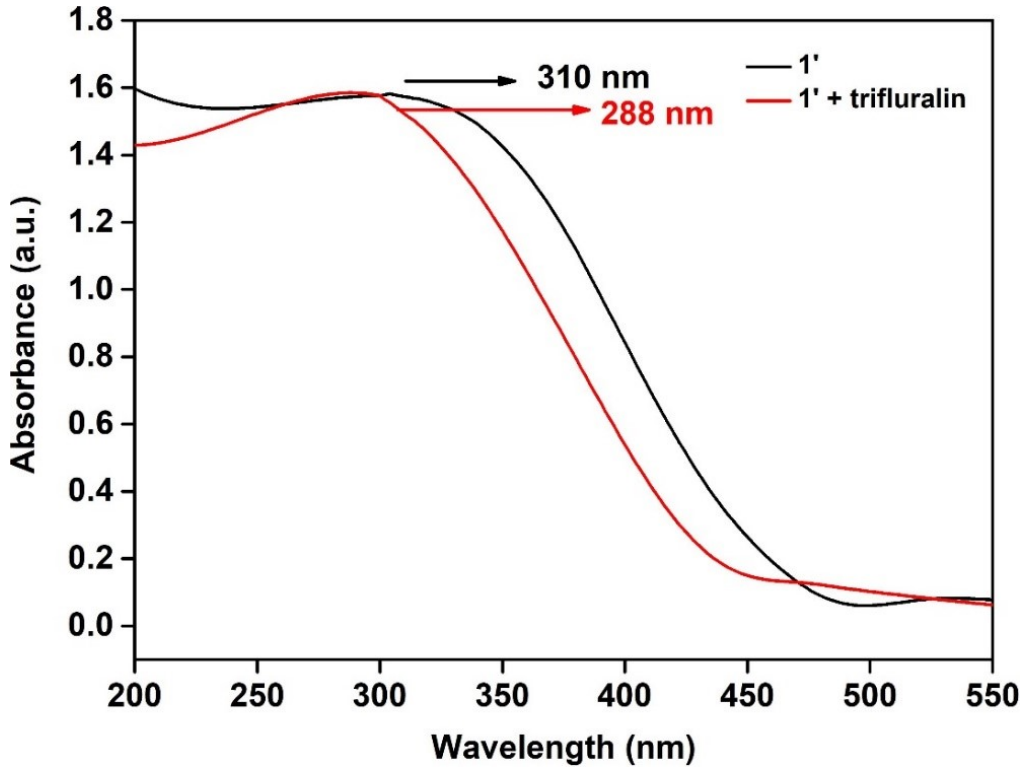

Fig. S48. Solid-state UV-Vis spectra of **1′** (blue line) and **1′** after sensing of trifluralin (red line).

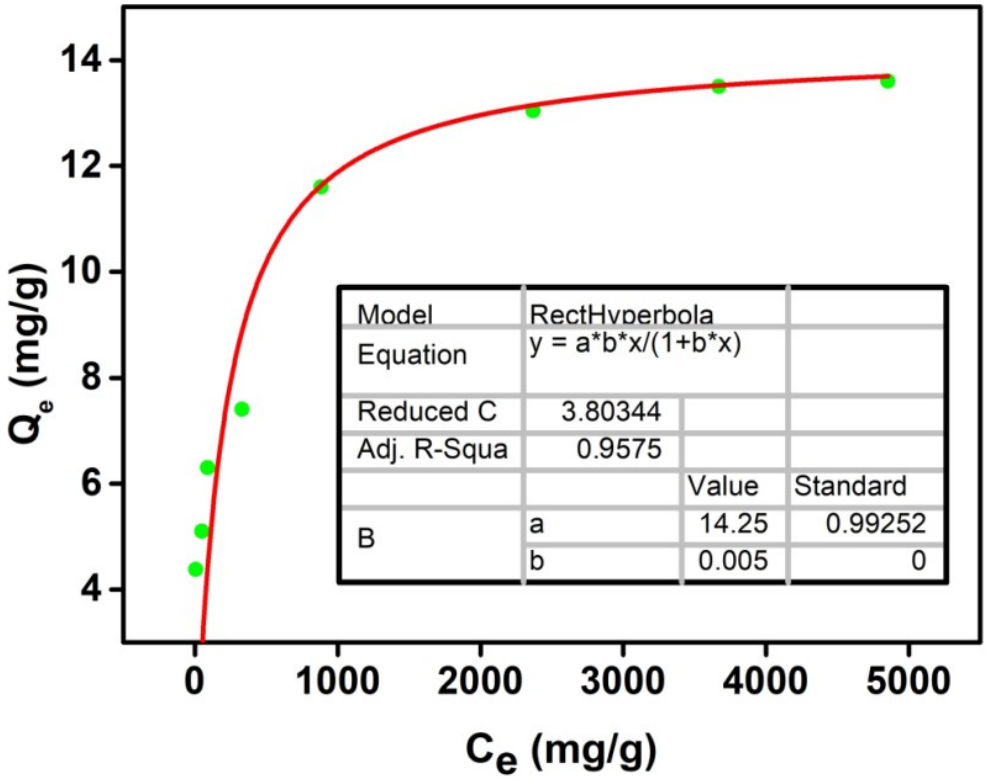

Fig. S49. Fitting of adsorption results of trifluralin in native fabric using the Langmuir model.

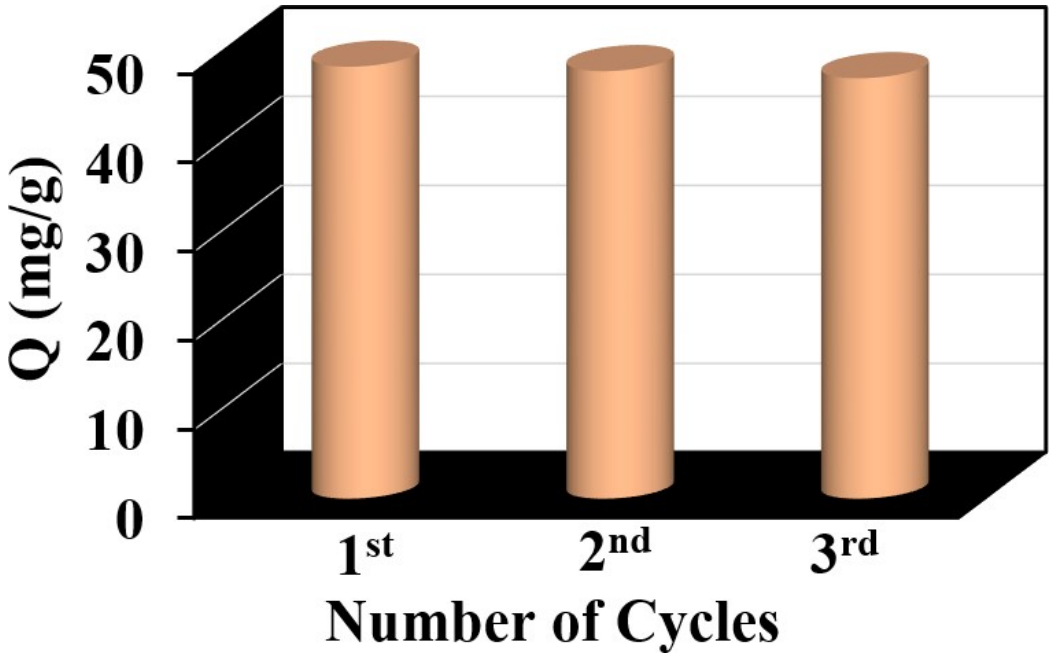

Fig. S50. Reusability of **1′**@cotton@starch composite for the adsorption of trifluralin.

References:

1. M. J.Frisch, G. W.Trucks, H. B.Schlegel, G. E.Scuseria, M. A.Robb, J. R.Cheeseman, G.Scalmani, V.Barone, B.Mennucci, G. A.Petersson, H.Nakatsuji, M.Caricato, H. P. H. X.Li, A. F.Izmaylov, J.Bloino, G.Zheng, J. L.Sonnenberg, M.Hada, M.Ehara, K.Toyota, R.Fukuda, J.Hasegawa, M.Ishida, T.Nakajima, Y.Honda, O.Kitao, H.Nakai, T.Vreven, J.

A.Montgomery, Jr., J. E.Peralta, F.Ogliaro, M.Bearpark, J. J.Heyd, E.Brothers, K. N.Kudin, V. N.Staroverov, R.Kobayashi, J.Normand, K.Raghavachari, A.Rendell, J. C.Burant, S. S.Iyengar, J.Tomasi, M.Cossi, N.Rega, J. M.Millam, M.Klene, J. E.Knox, J. B.Cross, V.Bakken, C.Adamo, J.Jaramillo, R.Gomperts, R. E.Stratmann, O.Yazyev, A. J.Austin, R.Cammi, C.Pomelli, J. W.Ochterski, R. L.Martin, K.Morokuma, V. G.Zakrzewski, G. A.Voth, P.Salvador, J. J.Dannenberg, S.Dapprich, A. D.Daniels, O.Farkas, J. B.Foresman, J. V.Ortiz, J.Cioslowski and D. J.Fox, Gaussian 09, Revision D.01, Gaussian, Inc., Wallingford CT, 2013.

2. J. H. Cavka, S. Jakobsen, U. Olsbye, N. Guillou, C. Lamberti, S. Bordiga and K. P. Lillerud, *J. Am. Chem. Soc.*, 2008, **130**, 13850-13851.
3. J. Wang, T. Xia, Z. Lan, G. Liu, S. Hou and S. Hou, *Spectrochim. Acta - A: Mol. Biomol. Spectrosc.*, 2021, **259**, 119880.